Mineral Spectra Extraction and Analysis of the Surface Mineralogy of Mars with Hyperspectral Remote Sensing

Mohit Melwani Daswani

March, 2011

Course Title: Geo-Information Science and Earth Observation for Environmental Modelling and Management

Level: Master of Science (MSc.)

Course Duration: September 2009 – March 2011

Consortium partners: University of Southampton (UK)
Lund University (Sweden)
University of Warsaw (Poland)
University of Twente,
Faculty ITC (The Netherlands)
GEM thesis number: 2011–

Mineral Spectra Extraction and Analysis of the Surface Mineralogy of Mars with Hyperspectral Remote Sensing

by

Mohit Melwani Daswani

Thesis submitted to the University of Twente, faculty ITC, in partial fulfilment of the requirements for the degree of Master of Science in Geo-information Science and Earth Observation for Environmental Modelling and Management

Thesis Assessment Board

Chairman: Prof. Dr. Freek van der Meer
External Examiner: Dr. Jadu Dash
First Supervisor: Dr. Frank van Ruitenbeek
Second Supervisor: MSc. Wim Bakker

Disclaimer

Abstract

The images acquired by the Observatoire pour la Mineralogie, l'Eau, les Glaces et l'Activité (OMEGA) hyperspectral spectrometer on Mars Express of the surface of Mars are affected by noise and large pixel sizes. The stability of the spectra used to identify mineralogy with OMEGA has not been studied in detail across different scenes and spatial resolutions. A modified image processing method and an analysis of correlation between spectra is proposed to evaluate how selected image spectra of key rock-forming minerals relate across different OMEGA image resolutions and to laboratory measurements of mineralogical spectra.

The Nili Fossae region at the western edge of the Isidis impact basin on Mars was the area chosen to be studied due to the diverse mineralogy that has been associated with it. Here, spectra were extracted from regions identified with spectral parameters or summary products where groups of rock-forming minerals occurred. Image-extracted spectra were used as endmembers to produce a spectral library with which the statistical method of spectral angle mapping was applied to map the mineralogical distribution in OMEGA images of different resolutions. The extracted spectra were also compared to laboratory spectra via their spectral angles.

Results showed low angles and high correlation between the extracted spectra in different resolutions, and relatively low correlation between the extracted spectra and the laboratory spectra. Spectral angle mapping of the images revealed that some spatial coherence of the mapped mineralogy existed, but spectra from the maps were highly correlated for all endmembers. A cross-validation between processed images from OMEGA and the higher resolution Compact Reconnaissance Imaging Spectrometer for Mars (CRISM) on NASA's Mars Reconnaissance Orbiter showed relatively low correlation between their corresponding mineral spectra. Visual identification of mineralogical spectra was more precise at identifying mineral species than summary products were.

Extracted spectra were stable across different resolutions but were not identifying precise minerals based on their spectral properties because the chosen summary products are not effective at identifying precise mineralogical spectra.

These summary products should therefore be used with care in future mineralogical analysis of Mars' surface with remote sensing. Spectra behaves stably enough across different resolutions, but with OMEGA, it would be best to use spectral angles to map with a library of minerals confirmed to be present by rovers, the direct sensors on the surface.

I would like to thank my ever supportive family and GEM family, friends at home, friend who actually came to visit (Mario), hosts (Rajesh, Pawel, Imma & Juliá, Joan, Jordan & Tommy), and also all the other faces - family, friends and housemates, some new, some old - I met along the way during this adventure (Meritxell, Federica, Vishal, Romina, Vanessa, Andrew, Marlena, Joanna, Csilla, Charlene, Kay Key, Jon and Louis).

A special thanks goes to Roderik Koenders (University of Delft), Tanja Zegers (University of Utrecht) and Agustín Chicarro (ESTEC - ESA), for organising the Landing Sites for Exploration Missions workshop at Leiden and Noordwijk (January 2011). That was a real eye-opener.

Finally, I would like to thank all my teachers and the staff at all the participating MSc GEM universities, the great students at ITC (too many to name!) and Louise van Leeuwen, our MSc coordinator. Oh, and my supervisors (Frank van Ruitenbeek and Wim Bakker) too!

Happy reading. I encourage you to be (constructively) critical - it can only help science.

All documents, data and analyses are digitally available from the author (i.e. me), who would be happy to facilitate it to anyone who so wishes to make use of it.

Contents

List of Figures

List of Tables

Chapter 1

Introduction

The European Space Agency (ESA)'s visible and infrared hyperspectral spectrometer Observatoire pour la Mineralogie, l'Eau, les Glaces et l'Activité (OMEGA) on the Mars Express (MEx) satellite has captured the spectral signatures of most of Mars' surface in varying spatial resolutions since it began orbiting Mars towards the end of 2003 [4].

Hyperspectral imagery from OMEGA has aided in mineralogical mapping of the Martian surface [23], [32] but due to its relatively low spatial resolution, resulting maps are often open to interpretation and a subject of discussion. To complicate matters, several other issues affect the OMEGA datasets, including noise and less than optimal calibration [3].

Aside from the problems arising due to the spectrometer, there are also limitations in the current models of Mars' atmosphere and solar illumination conditions [3] which have an impact on the interpretation and correction of OMEGA images, though these simplified models will not be altered in this project.

This MSc thesis aims to devise a method to extract useful spectral information from the images captured by OMEGA, investigate its usefulness for the correct identification (with respect to laboratory measurements) and mapping of surface mineralogy, and to understand the stability of spectra extracted OMEGA images across different resolutions and scenes. This information may then be used for geological interpretation.

The area studied is Mars' Nili Fossae region, which is of particular interest due to the diverse mineralogy confirmed to be present in it [21], [16].

1.1 Background

At the present moment, ESA's Mars Express (MEx) and NASA's Mars Odyssey and Mars Reconnaissance Orbiter (MRO) are the only working satellites orbiting Mars [7] and acquiring atmospheric and surficial information. All three are ageing satellites which have surpassed their intended lifetime, and neither ESA nor

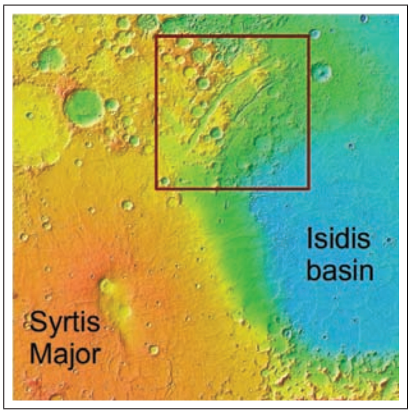

Figure 1.1: Elevation image of the Nili Fossae region (delimited by a 10° × 10° box) acquired Mars Orbiter Laser Altimeter on NASA's Mars Global Surveyor satellite.

NASA have planned orbiters to replace them in their entirety the near future. The joint NASA/ESA Mars Trace Gas Orbiter (TGO) is the only intended orbiter for Mars within the coming decade [7] and will gather detailed information on atmospheric composition, but will not carry a hyperspectral instrument for measuring the spectral properties of the surface.

Despite this, the wealth of hyperspectral data gathered by MEx/OMEGA as well as NASA's Compact Reconnaissance Imaging Spectrometer for Mars (CRISM) on MRO does not fall short, having imaged all the Martian surface[1]. The data gathered by both spectrometers served to discover and confirm the presence of hydrated minerals and clays [16] which were suspected to be present, as well as carbonates [19] and widespread mafic minerals [20]. Numerous articles [4], [22], [24] claim encountering the spectral signatures of very specific minerals (see sections 1.1.1 and 1.1.2) across the OMEGA hyperspectral datasets in spite of the abundant problems the latter faces, such as noise (see section 2.1.1).

1.1.1 Geology of Nili Fossae

The Nili Fossae region was chosen as the area of study interest for this thesis.

Current knowledge of the geology of Nili Fossae stems from studies that have confirmed Nili Fossae as a region of interest with spectral signatures indicating diverse mineralogy with OMEGA [4], [21], [16]. This diverse mineralogy was the main reason for choosing the Nili Fossae area as the area of study interest (approximately bound between 17° and 27° latitude and 71° and 81° longitude) (figure 1.1) However, the specific interpretations of the spectral signatures for mineralogical mapping with OMEGA remains a complex task and an issue of debate due to intrinsic difficulties in the nature of the data, the necessary corrections and preprocessing of the images prior to interpretation and the errors (discussed in section

---

[1] Raw data available at ESA's Planetary Science Archive for OMEGA (http://www.rssd.esa.int/index.php?project=PSA&page=mexIndex) and NASA's Planetary Data System (http://pds-geosciences.wustl.edu/missions/mro/crism.htm)

1.1.2) associated with the spectrometer. A workaround making use of spectral unmixing has recently taken some form to reduce the effect of the low spatial resolution [9], and to be able to identify the mineralogical diversity, which ranges from rare unweathered carbonates [10] to mafic silicates [4], clays and minerals resulting from aqueous alteration [16].

The prevalent interpretation of the interpretation of the Nili Fossae region based on superposition and relationship between geological units [21] describes units bearing the mineral olivine as contemporaneous to the Isidis impact (late Noachian age, approximately 3.96 Gyr ago) to the East of Nili Fossae. The olivine bearing rocks are found due to crustal melt and exposure from the impact, and the impact itself reveals subsurface crustal mineralogy [21] . However, phyllosilicates and hydrated minerals found to be present in the region are due to the presence of water, weathering and alteration of the bedrock associated with it prior to the impact event [16], and possibly due to fluvial and lacustrial sedimentary processes taking place in impact craters [13]. Conditions for weathering and production of hydrated minerals have not occurred since [16], when the Syrtis Major shield volcano in the vicinity of the Nili Fossae region was active and ejected lava flows containing dark, mafic minerals [20] (in the Hesperian period around 3.7–3 Gyr ago according to crater counts) [6].

1.1.2 Overview of the OMEGA spectrometer and a review of methods

The OMEGA imaging spectrometer on MEx forms part of a current and ongoing European initiative which has exceeded its expectations in relation to the sheer amount of data collected and science derived MEx reflected a trend at ESA to quickly construct effective space-bound instruments based on previous and ongoing missions and to reduce costs. OMEGA derives from a spare OMEGA spectrometer for Russia's Mars 96 mission [5] (the direct predecessor to Mars Express which failed during launch) and the electronics for power and control were based on the ÇIVA slash ROLIS instrument [5] (a CCD camera/spectrometer for Rosetta's lander set to arrive comet 67P/Churyumov-Gerasimenko in 2014) [11]. The scientific return has been nothing short of remarkable, and reflecting that, ESA's Science Programme Committee has extended the MEx mission four times so it will remain operational till at least December 2012, if it remains in stable orbit for as long.

OMEGA has been gathering hyperspectral images in 352 contiguous channels in wavelengths between 0.38 and 5.1 μm since January 2004. OMEGA is actually composed of two separate spectrographs: Visible to Near Infrared (VNIR) and Short Wave Infrared (SWIR). The latter in turn is formed by two spectrometers (SWIR1 and SWIR2) with a spectral overlap between them [12] (see table 1.1). Spatial resolution is varied between 0.3 and 4 km/pixel, depending on the area surveyed and the orbital characteristics of MEx. Images of all of Mars' surface were acquired fairly quickly at lower resolutions, providing spectral images on a global scale for the first time [4]. However, the fairly large pixel size is both an advantage and a disadvantage. On one hand it is easier to understand large scale implications

Table 1.1: OMEGA's sensors and spectral ranges.

Sensor	*Range (μm)*
VNIR	0.38–1.05
SWIR1	0.93–2.73
SWIR2	2.55–5.1

of the underlying geology and to see large spatial patterns and distributions should they exist, but on the other hand specific mineralogical detail and compositions as well as diagnostic structures and formations may be missed.

Yet another cause for concern related to the large pixel size is the actual interpretation of the spectral images: diverse mineralogy falling within the area covered by a pixel is grouped and results in a mixed pixel with a single spectral value. Recent studies [8], [33] have borrowed from image processing techniques used to unmix pixels on Earth-pointing spectrometers to obtain apparently reliable proportions of mineralogical compositions, but have been restricted to moderately effective methods such as linear spectral unmixing models, with all its limitations, e.g. assuming the surface imaged has no intimate mineral mixes but areal mixtures (linear combinations of minerals). The difficulties with this latter method include the need to define representative rock-forming minerals (and water ice) as endmembers expected to be found on Mars and identifying their spectral signatures, which is a difficult task given the need to extrapolate the known spectral signatures of minerals measured in controlled laboratory conditions to the spectral signature for the same mineral on Mars. This is a serious impediment to the technique due to the fact that a different instrument in different conditions has been used to carry out the task of identifying spectra which will be used as a spectral database or library to compare with OMEGA's obtained data. So far, these studies ([9], [15], [33]) have been able to identify the presence of mineralogies with some confidence but not their exact proportions, nor, as far as I have observed, have they evaluated the changes in spectra across scenes and the effect of the different resolutions of OMEGA.

Other approaches in tackling the problem of ambiguity in the information given by pixels and sub-optimal calibration provide good insights into what can be accomplished and integrated to form a more reliable processing model using image spectra. These include object-based segmentation [32], in which contiguous pixels with low variance between their characteristic absorption features are grouped; use of ancillary Thermal Emission Spectrometer data on NASA's Mars Global Surveyor satellite [18] to compare the suitability of specific spectral ranges to detect certain mineralogies; and similarly, the use of MRO's CRISM [22], which in contrast to OMEGA, has a very high spatial resolution (from approximately 20 to 200 meters/pixel, depending on the mode of operation and orbit) and convenient spectral summary products that can quickly parametrise a number of mineralogies, gasses and ice compositions [22].

This thesis relates to the mentioned sources by drawing from them (and especially [4], [22] and [3]) to follow a method to understand the spectral characteristics of OMEGA imagery and the relationship the image spectra has with mineralogy. It should be noted that two general groups of methods for characterisation of OMEGA spectra have been described for mapping mineralogy:

- Using a spectral library/database of a priori mineral spectral measurements and fitting this spectra to the image's spectra.

  And:

- Extracting spectra from the images themselves to build a spectral library, where relating to known mineralogical information is secondary, thus obtaining a higher relation between maps and spectra.

The mentioned unmixing techniques and cases in which there was use of ancillary data have introduced variations to the methods in order to improve them. This thesis follows the second method, since relating OMEGA's image spectra to mineralogical spectra might not be ideal due to the differences in conditions and instruments used for measuring in both cases.

1.2 Justification of research

Learning about Mars' geology will not only aid our comprehension of Mars' origin but also advance further understanding of our own planet, and indeed, any terrestrial planet through comparative studies. Mineralogical mapping of the surface of Mars will aid it's exploration and is useful for characterising landing sites and sites of interest for ESA's and NASA's planned joint rover and probe missions in the near future in view of attempting to study Mars' present and past, and to find traces of present or past life should it have existed.

On a more utilitarian and current view, the research will bring further understanding of how to identify mineralogy through hyperspectral remote sensing, and aims to comprehend how spectra are related to mineralogy. Concretely, the study will determine the response of OMEGA hyperspectral data in different scenes across the Nili Fossae region, known for being a diverse site of scientific interest and as a potential landing site.

1.3 Research questions and objectives

In a broad sense, this project aims to aid in the understanding of the geology of Mars. In order to do so, the issues with the tools used for the study the geology of Mars need to be addressed.

Previous studies have used spectral signatures of minerals in laboratory conditions as spectral libraries or databases to determine the nature of the spectral signatures in OMEGA images. However, due to the unreliability of using in-situ validation (or ground truth) and instrumental and conditional differences, direct comparison of OMEGA image spectra to laboratory spectra is uncertain. The following thesis begins with the hypothesis that spectra extraction from the OMEGA images directly (post-processing) without relying on external spectral library spectra is more veritable and therefore more useful to determine mineralogy. This does not mean that it is not useful to examine and contrast the spectra acquired from images with mineral spectra in laboratory conditions, but that spectra from both are not initially comparable, so it is erroneous to assume that spectra for the same minerals will have the same aspect in both cases. This fact, together with the comparison of the effects image resolution has on spectra and the cross-validation using CRISM, is what sets this research apart from previous attempts to understand spectral variation of OMEGA images.

The work carried out in this thesis intends to answer the following research questions:

- How can we adapt the OMEGA image preprocessing model to extract useful spectra from OMEGA hyperspectral imagery itself?
- Which specific mineral spectra (endmembers) should be chosen for mapping purposes?
- What is the stability of OMEGA hyperspectral spectra to identify specific minerals like?
- Are the spectra affected by the different image resolutions of OMEGA?
- Can a mapping method be used to map the mineral distribution and evaluate the spectral extraction method?

  And finally:
- How useful are the spectra for identifying minerals, compared to laboratory measurements of minerals?

The basic objectives followed to provide verifiable answers to these questions were:

- To review the current OMEGA image processing model in order to extract useful spectra; and build a spectral library of spectral endmembers from and for each of the images being studied.
- To statistically compare (validate and study the variation of) OMEGA spectra to identify minerals across different scenes and spatial resolutions using spectral angles (method discussed in detail in chapter 2.3).
- To statistically evaluate the spectra to identify minerals on OMEGA images with respect to laboratory measurements (again, calculating their spectral angles).
- To map the mineralogical endmembers extracted from the images through a statistical method (spectral angle mapping) and visually evaluate the spatial

coherence of the mapped regions, also by draping the maps over an elevation model.

- To check whether the particular conditions that occur in OMEGA images are exclusive to the OMEGA sensor or whether they occur on CRISM (an instrumental cross-validation).

Chapter 2

Methods

The following methods aim to answer the questions presented in chapter 1.

2.1 Methods to assess the OMEGA preprocessing and calibration model

To be able to assess the current preprocessing model for OMEGA hyperspectral images and find its limitations and points where it might be improved, a review of the model was carried out. In the proposed method, three test OMEGA images of the Nili Fossae region in different spatial resolutions were preprocessed, and the resulting reflectance spectra for selected minerals (Table 2.1) were visually compared to library spectra of the same minerals measured in laboratory conditions (United States Geological Survey (USGS) spectral library [8]). Mineralogical spectral libraries have often been used in visual comparative studies of observed OMEGA image spectra as a form of validation (e.g. [4], [21], [23]). Carrying out his method will help answer the question of whether improvements can be made to the preprocessing and calibration in order to obtain mineralogical spectra, and if so, which, and how can they be integrated in the current model.

The materials needed to follow the method were:

- OMEGA image datasets ORB3047_5 (high resolution), ORB2272_4 (medium resolution) and ORB0422_4 (low resolution). These were obtained from ESA's Planetary Science Archive (PSA) via FTP access and PSA's Java platform map-based searcher for Mars datasets.
- SOFT05, the OMEGA science team's software in IDL for calibrating OMEGA images [17]. SOFT05 was also obtained from the PSA.
- Alpha, a graphical user interface (GUI) for SOFT05 by van der Werff [31].
- IDL Workbench 7.1, to use SOFT05 and Alpha.

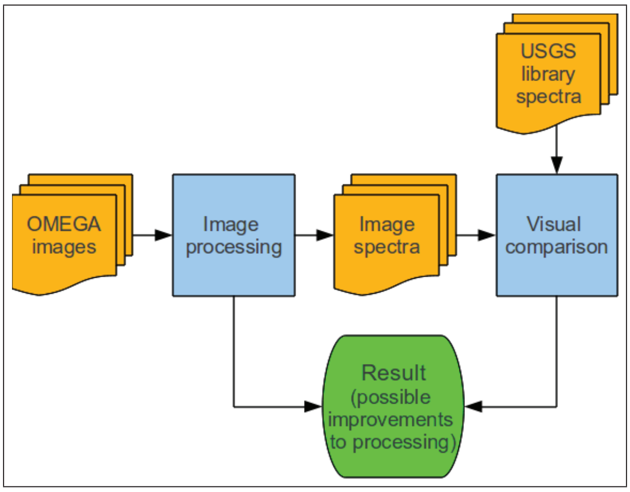

Figure 2.1: Workflow of the method to review the image processing model.

- PyENVI a software program developed in Python language for the purpose of viewing and processing images, which also implements a number of preprocessing corrections designed for OMEGA images [2].
- USGS splib06a digital spectral library.
- ENVI 4.7 software for processing and visualising images.

The workflow of the method is schematised in Figure 2.1.

2.1.1 The OMEGA preprocessing model

Following is a description of the current preprocessing strategy used for OMEGA hyperspectral images that were followed in order to review adjust it.

Due to the noisy nature and problems of OMEGA's raw data (discussed further in this section), image preprocessing is a necessary step prior to extracting spectra from them. The data must undergo a series of corrections for the spectra extracted to be useful for identifying signatures specific to selected minerals, so a processing standard is needed to handle the correction of data. These preprocessing corrections are equivalent to those used for hyperspectral remote sensing and characterisation of surface mineralogy on Earth, with the difference, however, that they are particular to the Martian conditions and more specifically the OMEGA instrument.

The basis of the preprocessing used in this project was devised by Bakker et al. [3]. Figure 2.2 summarises the preprocessing in a flowchart (up to obtaining useable images for preprocessing in order to gain mineralogical information.

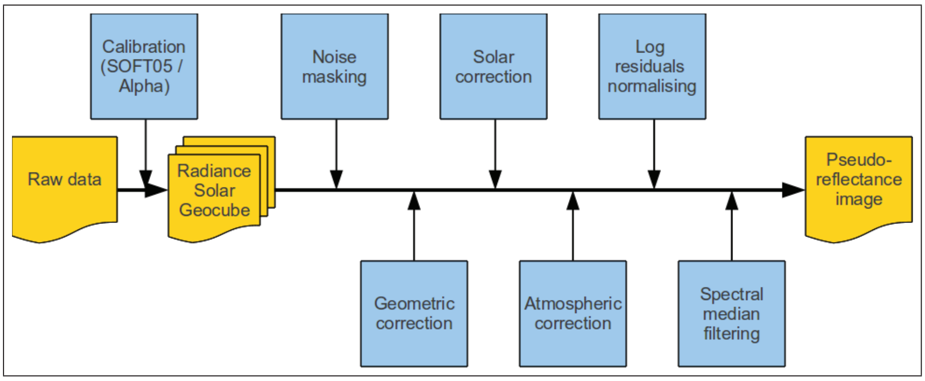

Figure 2.2: Flowchart summarising the preprocessing chain, adapted from the processing chain by Bakker et al. [3].

Raw data and calibration

ESA provides OMEGA's raw data for each dataset in the form of two files: one containing spectral information gathered by the OMEGA sensors ("datacubes" in .QUB files) and the other containing the geometric information about the geographic positioning of the images (in .NAV files). Using the SOFT05 calibration software developed by ESA for OMEGA's data in IDL, a 3 dimensional (in X and Y space degrees, and the spectral dimension in $W/m^2/steradian/\mu m$) radiance image of the dataset is obtained [17]. An inspection of the data shows that the spectral dimension is not given in irradiance units as claimed by the SOFT05 documentation, but is in fact a measure of spectral intensity. Other data files are obtained from the calibration software for each dataset, including a geocube file with geographic information, and the solar spectrum at the distance of Mars at the time of the acquisition of the image.

Noise reduction

Noise is apparent throughout raw OMEGA radiance images. The nature of the noise is varied, consisting of banding and stripes; dead (i.e. with no values), hot or defective (i.e. with constantly high values) pixels; bad channels; and degradation of the signal in later datasets. The possible origins of the noise are not covered in the scope of this project, but are largely due to calibration issues, instrumental failure in OMEGA, problems in data transfer to Earth, orbital decay of MEx and exposure to cosmic radiation in time, among other possible reasons [17]. Displaying uncorrected radiance images shows that out of the three, OMEGA's VNIR and SWIR2 spectrometers are the sensors most affected by noise throughout. Additionally, the SWIR2 sensor's spectral signal is affected by thermal effects as it approaches longer wavelengths, especially beyond 3.5 μm.

Calibration carried out by SOFT05 accounts for the known unreliable hot and dead pixels [17], but most noise in the radiance images was corrected after the separation of the sensors' spectral ranges of the individual datasets by masking the wavelength bands most affected by it [3]. Masking these bands has the effect of removing the noisy bands from further analysis and corrections where they would affect neighbouring useful bands. Masking spectral bands is carried out in PyENVI and is a general method of determining useful ("good") bands which will be suitable for further processing and useless ("bad") bands which will be rejected from processing and analysis and are considered to not bear information. Masking applies the signal to noise ratio to determine an acceptable output by adjusting a threshold. The downsides to this procedure are the increased time consumption and possible reduction of information, however, the benefits far outweigh the disadvantages, as it outputs reduced but cleaner data.

Preprocessing corrections

The remaining preprocessing corrections were carried out in PyENVI.

The datasets are geocorrected individually employing the geocube extracted by SOFT05 from the raw OMEGA files. The resulting images undergo a standard solar illumination effects correction with the solar spectrum derived also from the calibration of the raw data with SOFT05.

Following the preprocessing chain (figure 2.2), an atmospheric correction was carried out on the individual datasets. The atmospheric correction is a standard and general function applied to all bands under $3.5\mu m$ of the atmospheric transmission derived from the difference between the spectrum measured at the summit of the Olympus Mons volcano (the highest point on the surface of Mars) and the base of it, assuming a power law variation of the transmission with altitude [20]. The result of these corrections are images consisting of absolute reflectance values.

The resulting absolute reflectance image is not exempt from all noise and other effects, but these are largely corrected through normalisation with log residuals with a geometric mean of the image, assuming the scene is heterogeneous [2]. As a consequence of this last correction, the spectral signature is converted to pseudo-reflectance. Subsequently, a hyperspectral median filter is applied to the images to further smooth them. Again, this is achieved in PyENVI, where each pixel in the image is computed as the median of its value and the pixel values directly adjacent to it (figure 2.3). This achieves the effect of preserving edges and spectral features while reducing the overall noise [2].

Mineral abundance and distribution

In order to obtain information on the abundance of specific minerals MRO/CRISM spectral parameter summary products based on band depth ratios [22] are adjusted to OMEGA's bands and used to identify a selected mineralogy. Table 2.1 contains a list of the minerals and the criteria used to identify them.

To apply the summary products on the pseudo-reflectance images obtained after the preprocessing corrections, the convex hull of each pixel is removed via the

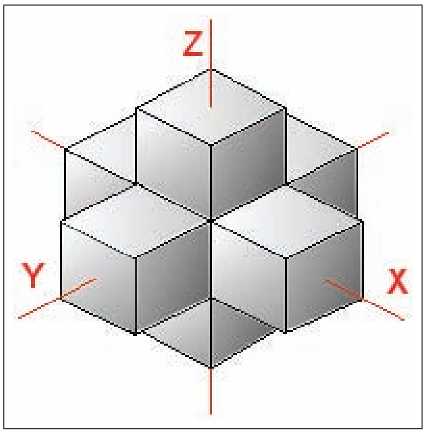

Figure 2.3: Median filter pixel window, 7 pixels in all, i.e. the central pixel and those in the X, Y and spectral (Z) dimensions.

continuum removal program in PyENVI for normalising spectra to 1 to apply the summary products of the hydrated minerals (D2300 and D2400) [2].

2.2 Method to select and extract spectra from endmembers

The results of the following method to choose and extract spectra from endmembers are entirely dependant on the results of the previous process to find and implement improvements in the OMEGA image preprocessing and processing model. The preprocessing model is necessary to obtain reflectance images of the surface from which spectral information of the mineralogy may be derived, so any changes affecting the model affect the spectra. However, the methodology to select and extract spectra itself is independent of the image preprocessing model.

To choose regions on the OMEGA images from which to extract representative endmember spectra, spatially overlapping scenes in differing spatial resolutions were used. As such, it was necessary to identify groups of datasets where a low resolution image contained or overlapped with a medium resolution image which in turn contained or overlapped with a high resolution one. This provided a form to confirm the validity of the spectral measurements at the same point.

The points within the overlapping images which corresponded to selected endmembers (and from which the spectra were extracted) were themselves found by identifying the highest values of each summary product (Table 2.1) and building regions of interest (ROIs) of these. Candidate areas for extracting spectra had to therefore have overlapping ROIs with high values in all three spatial resolutions.

It was considered that “high” values for each endmember were the highest 2% of values in each image. This percentage was chosen as a compromise for obtaining representative endmember spectra, yet safe from any outlier pixels that may affect the average extracted spectra. The percentage also offered certainty in some spatial cohesion of the high value pixels, and though a small portion of the image, ROIs

Table 2.1: The summary products to identify selected groups of minerals (adapted from [22]) used in this thesis to build a spectral library from image spectra. R is the reflectance and CR is continuum removed reflectance at specified wavelengths in nanometres (nm).

Mineral	*Name*	*Calculation*
Olivine	OLINDEX	$\frac{R1695}{0.1\times R1050+0.1\times R1210\times 0.4\times R1330+0.4\times R1470}-1$
High calcium pyroxene	HCPINDEX	$\frac{R1470-R1050}{R1470+R1050}\times\frac{R1470-R2067}{R1470+R2067}$
Low calcium pyroxene	LCPINDEX	$\frac{R1330-R1050}{R1330-R1050}\times\frac{R1330-R1815}{R1330+R1815}$
Carbonates	CINDEX	$R3750+\frac{R3750-R3630}{3750-3630}\times\frac{3950-3750}{R3950}-1$
Phyllosilicates	D2300	$1-\frac{CR2290+CR2320+CR2330}{CR2140+CR2170+CR2210}$
Sulphates	D2400	$1-\frac{CR2390+CR2430}{CR2290+CR2320}$

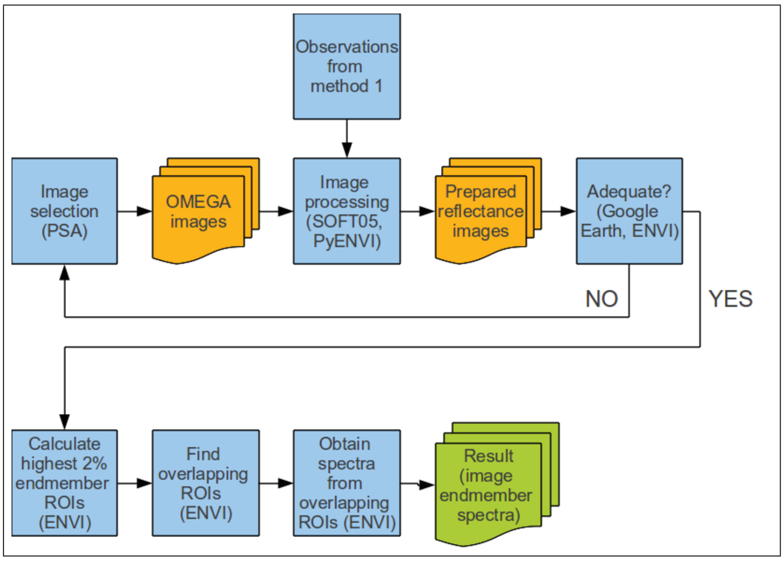

Figure 2.4: Workflow for selecting and extracting endmember spectra. The selection of OMEGA images and the adequacy of the processed images depends on whether the images spatially overlap, are of the Nili Fossae region and have differing resolutions.

formed from 2% of the highest value pixels are sufficient to visually identify ROIs overlapping with those of other images.

Materials used for selecting and extracting endmember spectra were:

- Java map-based Mars dataset searcher on the PSA.
- SOFT05 software.
- Alpha software.
- IDL 4.7 software
- PyENVI software.
- Google Earth software to visualise and choose overlapping images.
- ENVI 4.7 software for computing file statistics, creating ROIs and extracting spectra.

Figure 2.4 summarises the workflow of the method to select and extract endmember spectra.

2.3 Method to cross-validate endmember spectra across scenes

This method aims to answer how reliable spectra extracted from the processed OMEGA images are across different OMEGA observations. In this way, it is possible to determine whether the spectra is stable, or whether other unaccounted for factors intervene in the spectral observations. The method to compare endmember spectra in different scenes relies on the resulting spectra obtained in the previous method. The spectra extracted from each image across the Nili Fossae for each endmember was compared statistically. Normalised cross-correlation, or “spectral angle” (2.1), as it is referred to in remote sensing applications, was used as a measure to assess how well an endmember spectrum from one image fit with another spectrum of the same endmember, extracted from another image (overlapping or not). The spectral angle is ’a metric to measure “angular distances”’ [1], [27] in feature space, and can be used as a measure of correlation between multidimensional vectors (spectra, represented by v_1 and v_2). The larger the angle, the more uncorrelated and dissimilar the shape of the compared spectra are. It is especially useful for OMEGA hyperspectral images since it is mostly insensitive to magnitude (pixel brightness), but highly sensitive to spectral shape, patterns and features [29].

$$\text{Spectral angle} \quad \theta = \arccos\left(\frac{v_1^T v_2}{\|v_1\|\|v_2\|}\right)$$
$$\text{Where } v^T \text{ is the transpose vector and } \|v\| \text{ is the magnitude of the vector} \tag{2.1}$$

Spectral angles can be converted to correlation ($\cos\theta$) since the angle at which two compared spectra are completely unrelated is $\pi/2\,rad$ or $90\,^\circ$, and the angle at which they are correlated is close to $0\,rad$ ($correlation = 1$). The spectral angle was calculated between each of the selected endmembers and for a group of datasets in varying spatial resolutions (Table 2.2). Comparing the correlation between spectra extracted for different endmembers afforded a measure of how well the method for identification and extraction of endmember spectra performed. The selection of these datasets was purposive in the sense that they were representative of the Nili Fossae area. The group of images was composed of images of different resolutions which overlapped each other on some of their extents.

Table 2.2: Selected OMEGA datasets for spectral extraction and validation.

		High res.	**Medium res.**	**Low res.**
Name		ORB3047_5	ORB0232_2	ORB0444_4
Spatial res.		0.0075° lat ≈ 445m	0.017° lat ≈ 1Km	0.0601° lat ≈ 3.56Km
Geo. Extent	*Lat*	17.911 – 45.901	14.213 – 30.991	22.062 – 35.825
(Dec. degrees)	*Lon*	73.240 – 74.185	72.533 – 74.916	62.586 – 75.268

2.4 Method to cross-validate endmember spectra between instruments: OMEGA and CRISM

One CRISM reflectance image was selected from which endmember spectra was extracted following the same method as the OMEGA images (i.e. post-correction, using the CRISM summary products 2.1 and thresholding the highest 2% of values). Spectral angle was again used to compare between the extracted endmember spectra between images.

The CRISM image selected for comparison (HRL000095A2_07_IF183S_TRR2) was purposely chosen because it partially overlapped a high resolution OMEGA image (ORB3047_5) and the possibility that similarities might exist between them was observed. Despite this, their resolutions are very different (Table 2.3).

Table 2.3: Comparsion of OMEGA and CRISM datasets used.

	CRISM	**OMEGA**
Name	HRL000095A2_07_IF183S_TRR2	3047_5
Spatial res.	18.6 m	$0.0075^{o} \approx 445$m
Bands	430 (post-masking)	221 (post-masking)
Spectral range	1.02μm – 3.92μm	0.52μm – 5.09μm

To calculate the spectral angle, the number of bands and wavelengths compared must be the same, so the CRISM (of higher spectral resolution, but shorter range) was resampled to the OMEGA image (of lower spectral resolution, but longer range). This resampling order was important to avoid the extrapolation of OMEGA's lower resolution to higher resolutions. Only the converging spectral range between OMEGA and CRISM was used.

2.5 Method to compare spectra to laboratory measurements

To understand how useful the endmember spectra extracted from OMEGA images are to identify minerals, it was necessary to compare it to experimental observations of mineral spectra in controlled conditions. Adhering to standard, the USGS spectral library [8] was used as a visual comparison (as by [4], [21], [23]) with the image endmember spectra. Each extracted endmember spectrum was compared with its corresponding mineral spectrum statistically with their spectral angle. The angle between each extracted spectrum and the other candidate endmember spectra from the spectral library were compared to see whether similarities existed and whether errors in identification of ROIs and spectra in the images occurred.

The spectral library spectra (of higher resolution, shorter range) was resampled for each OMEGA image (lower spectral resolution, longer range), and only their common spectral range was used.

2.6 Method for mineralogical mapping and visual assessment of mineralogical distribution

The method for mapping is dependant on the endmember spectra extracted from the images (see 2.2) as it uses the spectra precisely as endmembers from which all surface mineralogy is formed or is a combination of. The chosen method for mapping was spectral angle mapping (SAM). The exact endmember spectra used for mapping each image were extracted from their respective images. Completed maps were draped onto Google Earth/Mars to be visually inspected for spatial coherence of the mapped mineralogy and to see whether relationships exist between topography and mineralogy.

2.7 Additional method to visibly compare spectral features

Due to obtaining some unexpected results (section 3.3 for the results and section 4.5 for discussion) after the application of the previously mentioned methods, it was necessary to understand whether the methodology suffered from a design flaw (specifically, the use of summary products) and to reevaluate a core component of the methods. In essence, the following hypothesis was tested: visual identification and comparison of the depth and position of spectral features in extracted spectra against random laboratory measured mineral spectra on a trial and error basis can provide comparable or better results than the summary products in relating to real mineral spectra. The test of the hypothesis consisted of the following:

1. Since the carbonate index summary product (CINDEX) identified a somewhat different spectral signature from the signature the other summary products identified (see sections 4.1 and table 3.2), its extracted spectrum for each of the resolutions was plotted.

2. The spectra extracted with the low pyroxene index formed part of the group of spectra that was generally indistinguishable from each other with spectral angle mapping. As a representative of this group, its spectra were also plotted in a separate plot as a group.

3. Each of the USGS spectral library spectra (481 in total) were plotted together with the CINDEX plots and LCPINDEX plots.

4. The continua of the spectra were removed to enable visual comparison of any spectral features.

5. Mineral spectra from the library were discarded based on how well their features compared visually to the extracted CINDEX and LCPINDEX spec-

tra, till only three candidate minerals remained, regardless of their plausible existence on the surface of Mars.

6. The spectral angle between the candidate minerals from the spectral library and the CINDEX and LCPINDEX spectra were calculated and compared to the spectral angles between the summary product spectra and library spectra in section 3.3.

Should the hypothesis prove to be true, then the summary products are no more effective at identifying spectral variations related to mineralogy than visual comparison of the spectral features. If the hypothesis is false, then the summary products are better at identifying mineralogical spectral variations.

Chapter 3

Results

3.1 Observations of the OMEGA image pre-processing chain

The results from the extraction of spectra using the unmodified image processing model revealed that mineralogical identification is not clear-cut. The process of selecting ROIs from where to extract mineral spectra showed that the pixels in the ROIs were spatially coherent and not randomly distributed (Figure 3.1), however, the spectra extracted from the ROIs tended to look similar within a dataset (despite being extracted from ROIs supposedly identifying different minerals) and different between datasets (despite supposedly identifying the same mineral) (confirmed in Section 3.3). In general, spectra from all scenes did not present noticeable absorption features which could be used to identify them easily by comparing them to mineralogical spectra (see results of the comparison between endmember and mineral spectra, Section 3.3). Stretching the spectra and observing only the SWIR1 range permitted the observation of a weak H_2O absorption feature at close to 1.9 μm, and no other distinguishable features with confidence.

Noise was present between the VNIR and SWIR1 bands in all datasets, but was especially noticeable in the medium resolution ORB2272_4 image because of the large jump in pseudo-reflectance between the VNIR and SWIR1 bands. The noise is an effect of ordering the bands according to their wavelength (since there is a spectral overlap between the sensors' bands) and very different readings between sensors. The reason for such different readings between sensors is unknown and is likely due to instrumental and/or calibration failure of OMEGA.

In particular, image spectra to identify olivine was only somewhat visually similar to the olivine library spectrum (Figure 3.2). The peak in the visible range is visible in the medium resolution image (ORB2272_4) but is absent in the other images. This peak may indeed be related to olivine spectra, but it is probably due to a calibration artefact in the mid-resolution image, since it is present in the extracted spectra of the other endmembers. The concave absorbing curve in the

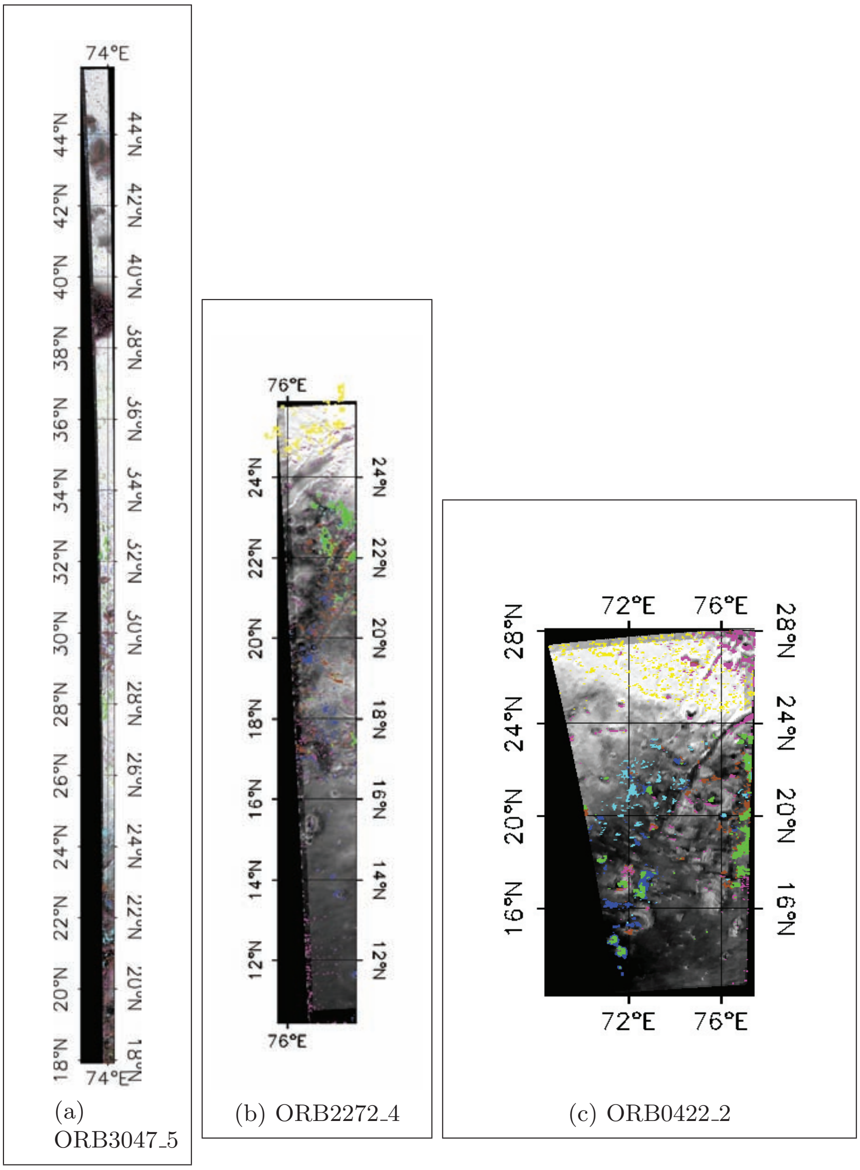

(a) ORB3047_5

(b) ORB2272_4

(c) ORB0422_2

Figure 3.1: ROIs draped over the studied reflectance images. Green: OLINDEX, cyan: LCPINDEX, blue: HCPINDEX, yellow: CINDEX, brown: D2300, magenta: D2400. ROIs were selected as described in Section 2.2.

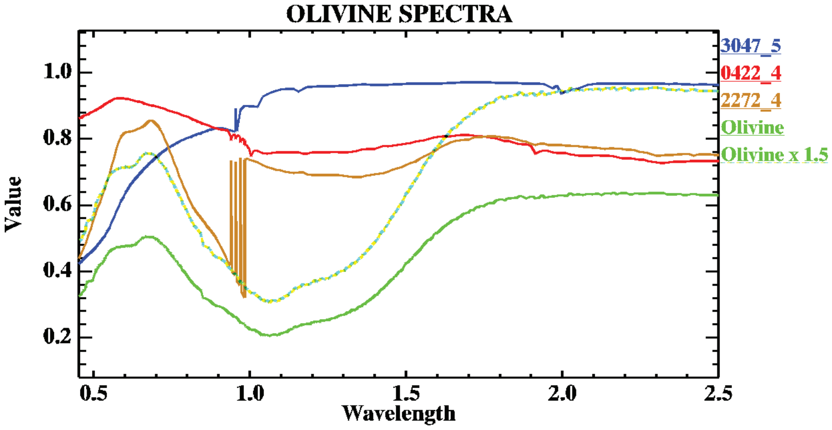

Figure 3.2: Pseudo-reflectance spectra from the olivine ROIs of the different resolutions compared to olivine spectra from the USGS spectral library.

NIR is also almost wholly absent in all datasets. All datasets conform to the library spectra from 1.7μm to 2.5μm as a featureless straight line.

Spectra from the ROIs were unsuccessful in their identification of low calcium pyroxene (Figure 3.3). Though having wide, featureless curves, the spectra did not harmonise with the curves of orthopyroxene (known as hypersthene in the spectral library) or any other low calcium pyroxene.

In the case of high calcium pyroxene, the ROI spectra were much more successful in following the spectral curve of diopside and especially, pigeonite (Figure 3.4). Although the pseudo-reflectance values of the extracted spectra and the reflectance values of the library spectra differed, the shape of the curve is similar and the values can simply be linearly rescaled to observe better fitting.

Though lacking the strong, characteristic absorption features at 1.4μm and 2.3μm of serpentine, the phyllosilicate ROI spectra performed moderately well in concurring with the general curved shape of some phyllosilicate library spectra, especially from the serpentine group (Figure 3.5). Serpentine's shallow, wide absorption close to 2μm was captured by the high resolution image (ORB3047_5), but the curve was better represented in the other two resolutions.

Regarding sulphates, the medium (ORB2272_4) and low (ORB0422_2) ROI spectra performed moderately well past 1.5μm in following the slight downward trend of the sulphate jarosite towards higher wavelengths (Figure 3.6). However, it is hard to see much similarity between the extracted spectra and the library spectra on wavelengths lower than 1.5μm.

Finally, for identifying carbonates, the ROI spectra only approximated the spectra of calcite between 1μm and 1.7μm. They did not present any of the characteristic absorption features of carbonates and remained mostly flat in SWIR1, though presented a peak in VNIR, inconsistent with carbonates (Figure 3.7). The

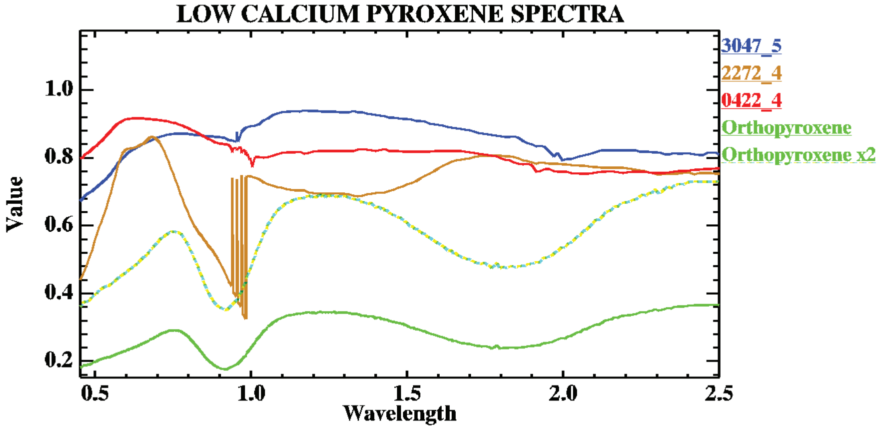

Figure 3.3: Pseudo-reflectance spectra from the LCP ROIs of the different resolutions compared to orthopyroxene spectra from the USGS spectral library.

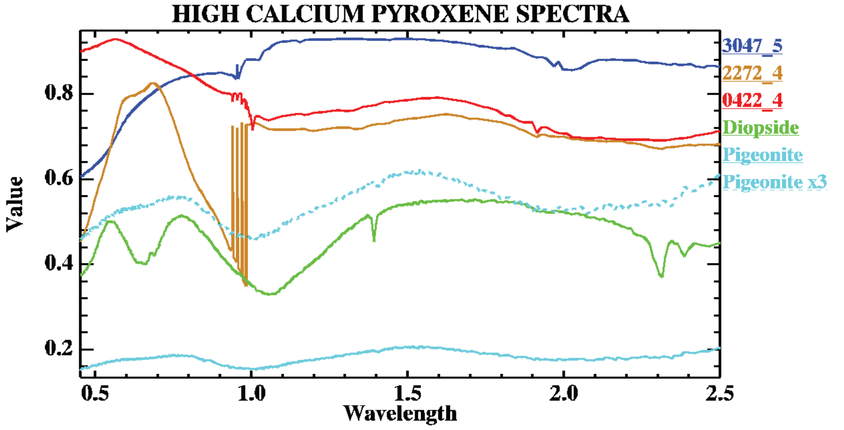

Figure 3.4: Spectra from the high calcium pyroxene ROIs
Pseudo-reflectance spectra from the HCP ROIs of the different resolutions compared to diopside and pigeonite spectra from the USGS spectral library.

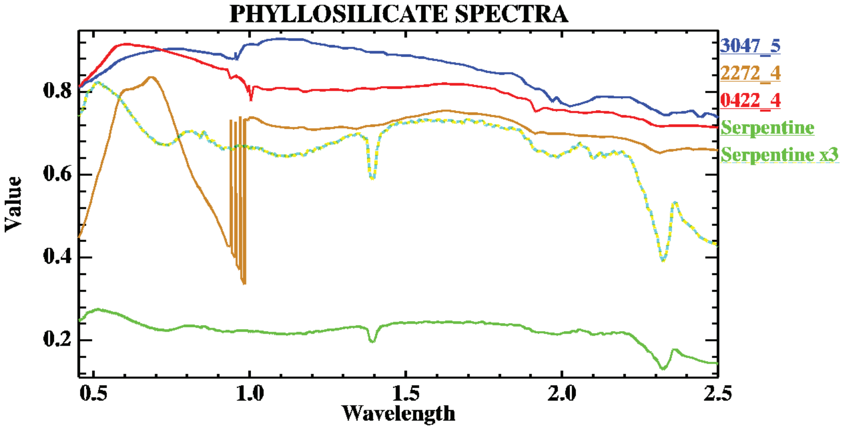

Figure 3.5: Spectra from the phyllosilicate ROIs
Pseudo-reflectance spectra from the phyllosilicate ROIs of the different resolutions compared to serpentine spectra from the USGS spectral library.

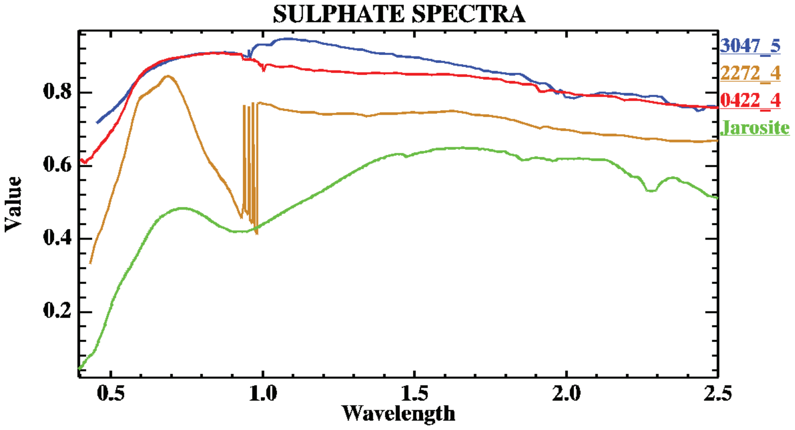

Figure 3.6: Spectra from the sulphate ROIs
Pseudo-reflectance spectra from the sulphate ROIs of the different resolutions compared to jarosite spectra from the USGS spectral library.

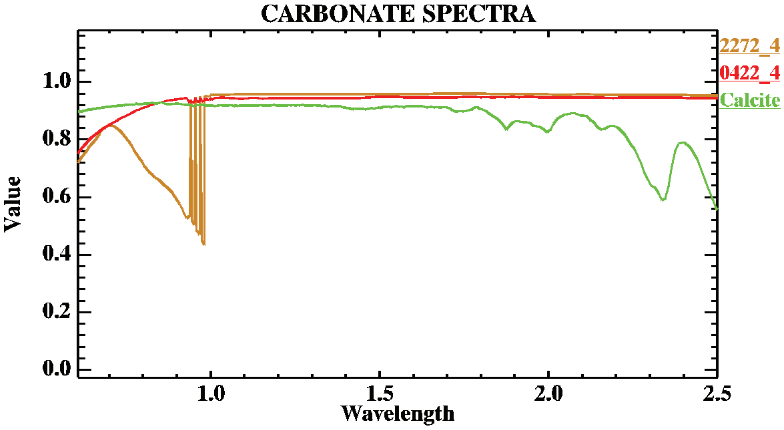

Figure 3.7: Spectra from the carbonate ROIs
Pseudo-reflectance spectra from the carbonate ROIs of the different resolutions compared to calcite spectra from the USGS spectral library.

CINDEX summary product for identifying carbonates could not be applied on the high resolution dataset (ORB3047_5) because the bands necessary for the product were considered “bad” and had been masked due to a low signal to noise ratio.

3.1.1 Concluding remarks on the preprocessing technique

Images obtained as a result of applying the processing chain were affected by the following issues:

- A general reduction of potentially useful bands as a result of applying the same signal to noise ratio threshold across all the sensors when masking noisy bands, especially at the beginning and the end of the sensor ranges. This meant that some summary products could not be applied always (e.g. CINDEX on dataset ORB3047_5).
- Modification of the real reflectance values due to applying log residuals on the image and normalising the signal across all the sensors. (As a consequence, image spectra were not easily and directly comparable to mineral spectra from spectral libraries, though they were visibly cleaner.)
- A spatial misregistration between the sensors is apparent, denoting that the geographic coordinates of every pixel differ between sensors.

Unknown factors independent of the preprocessing model also have an effect on the spectra obtained and complicate the identification of minerals. Other issues beyond the scope of the thesis such as the simplified atmospheric transmittance model and solar spectrum were not modified. But alterations to the original processing model were made in response to the mentioned list of known issues. Figure

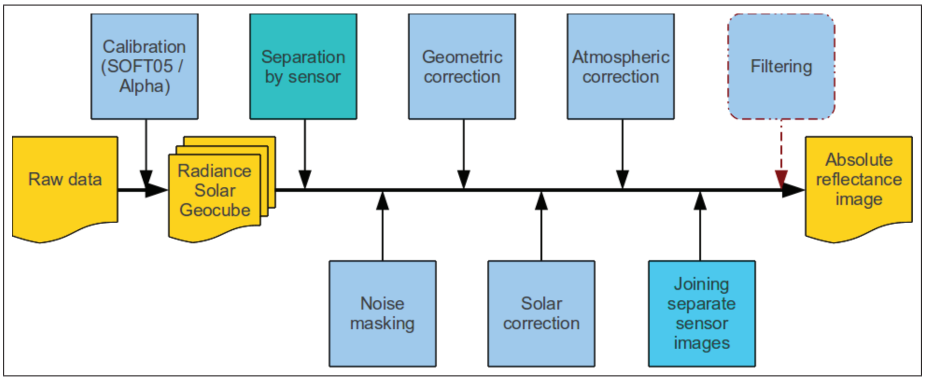

Figure 3.8: Flowchart summarising the pre-processing chain. Spectral median filtering is a process applied in specific circumstances, as described in Sections 3.2.4 and 3.2.5.

3.8 summarises the corrected preprocessing model in a flowchart, and Section 3.2.6 exemplifies the corrected processing method step by step with a dataset from the study area.

3.2 Improving the preprocessing methodology

3.2.1 Minimising spatial shifts

A noticeable problem occurring in OMEGA's spectral images (and left uncorrected till the analysis in this thesis) is the spatial shift existing between the different spectrometers' domains (Figure 3.9). This causes the geocorrection of primary images (which contain the complete spectral range of OMEGA) to be a source of error, as it produces alterations of the spectral signature throughout the image. To correct for this, all datasets were separately processed according to the sensors' spectral ranges (VNIR, SWIR1 and SWIR2). This is a decisive step away from previous processing methods for OMEGA's datasets, which had either focused on the SWIR1 range or at the most from $0.3\mu m$ to $2.5\mu m$ (e.g. [20], [23], [18]) and then attempted to extract useful information.

The separation was achieved by creating data subsets through the masking of the unrequired sensors' bands for each correction. The reflectance images of the separate ranges were joined after applying the preprocessing corrections into one image using an image to image registration process across the three images, by finding easily identifiable reflectance features (e.g. craters and distinguishable geomorphological features) i.e. pixels as tie points, across the images in different wavelengths. This post-correction joining process took advantage of the spectral overlap between the sensors (between VNIR and SWIR1, and between SWIR1 and SWIR2). The standard procedure followed was to start with the SWIR1 sub-

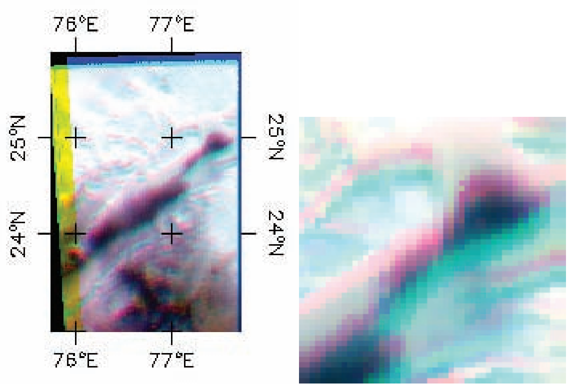

(a) Spatial shift (b) Close-up of the shift

Figure 3.9: Detail of the spatial shift between VNIR (blue), SWIR1 (green) and SWIR2 (red) in dataset 2272_4. Note the duplication of features (magenta and cyan) in the enlarged image on the right.

dataset as the base image (due to it being the least affected by noise) and warp the VNIR dataset to fit SWIR1's features and extent. The warped VNIR and the SWIR1 were stacked and used as the base image to warp SWIR2. SWIR2 was then stacked under the joint VNIR and SWIR1 image to form one single stacked image per scene with OMEGA's full corrected spectral range. The number of tie points chosen varied from scene to scene, dictated by their extent and spatial resolution, but the root mean square error (RMSE) associated with the selection of tie points was consistently maintained under 1, i.e. below the value of the cell size.

3.2.2 Further noise reduction

Noise was decreased by masking bad bands in the separate images in a process equivalent to the original preprocessing method (see 2.1.1), but as the raw image data is now divided according to the sensor that captured it (forming three separate images per dataset), the signal to noise ratio is different for each sub-dataset which is applied on a case by case basis for every sensor's range in a dataset to form a list of bad bands used for a mask.

Despite increasing the time needed to process images, it is advantageous because noise does not appear recurrently and equally among the three sensors.

3.2.3 Refined preprocessing corrections

The geographic correction module of PyENVI was carried out on the individual subset images (i.e. post-separation and prior to joining), the output of which was treated with the solar illumination correction and subsequently the atmospheric correction. This is analogous to the original preprocessing chain, with the difference that the corrections are applied on the images corresponding to the wavelengths of the individual sensors. In turn, this signifies that there is no mixing of data between the sensors. The resulting images consist of absolute reflectance values.

After applying the aforementioned corrections, the separate sensor images were joined as described in Section 3.2.1.

3.2.4 Post-joining preprocessing corrections

The joined image consists of absolute reflectance values and may be used for spectral analysis techniques and for extraction of spectra, however, as in the original preprocessing method, hyperspectral median filtering is applied as it is favourable in removing outliers in values while preserving edges in the images, and so reducing the overall noise.

Contrary to the initial preprocessing method, log residuals were not applied on the image to remove systematic errors because doing so resulted in altered reflectance values (pseudo-reflectance) not corresponding to spectra useful for magnitudinal comparison with actual mineral spectra.

3.2.5 Endmember spectra selection and extraction

After the preprocessing steps in the previous section have been carried out, the images' spectral signatures are useful for obtaining information about the mineralogy. A selected number of CRISM's mineral parameter summary products (Table 2.1), as described by Pelkey et al. [22] were applied on the preprocessed OMEGA scenes. To correctly apply the summary products, it was necessary to calculate log residuals after the atmospheric correction (instead of applying the median filter after the atmospheric correction) and then apply the median filter. This was done because each summary product identifies regions of the image for the presence of a mineral by quantifying each pixel, based on the summary product equations (Table 2.1), which are independent of the reflectance magnitude.

The continuum was then removed from each pixel. This was done in order to visualise and delimit the distribution of chosen minerals by using band ratios and spectral features specifically designed to detect the presence of these minerals (i.e. the summary products), and not for the extraction of spectra itself (for which having absolute reflectance was a better option in order to have absolute measures and statistical comparison). The choice of these minerals was decided on the importance of these as possible rock-forming minerals on the Martian surface and the combination of which could be mapped (endmembers, chosen with the summary products). The minerals in particular were well known groups of mafic minerals (olivine and pyroxenes) as well as carbonates, hydrated silicates and sulphates, with well known spectral characteristics as well as forming part of the mineralogy of many rocks on Earth.

Following the application of summary products on an image, regions of interest (ROIs) are created from the pixels with the highest 2% of values found by each of the summary products and are taken as acceptable spectral signatures to be included as endmembers in a spectral library unique to each image. The spectral library consists of all the mineral endmember spectra extracted from the images of the study area and functions as a database to which spectra from any processed OMEGA image may be matched against using a mapping technique (see Section 2.6).

Spectra for endmembers were collected from the ROIs in images of the Nili Fossae area at different spatial resolutions to acquire a representative sample for the spectral library. To evaluate the effect of the different spatial resolutions on the spectral signatures of the images, datasets with the three different spatial resolutions OMEGA is capable of (high, medium and low; depending on MEx's orbit) and spatially overlapping were grouped. ROIs of the highest 2% of values for the summary products were created for each dataset and compared to datasets within the same group to observe overlapping ROIs. Spectra from overlapping ROIs was in turn compared. As such, the effect of the different spatial resolution on OMEGA's images could be seen on endmember spectra extracted from the same location.

3.2.6 Procedure for preparing datasets and extracting spectra from overlapping datasets at different spatial resolutions

The following section describes the steps taken to obtain spectra derived from the OLINDEX summary product (the procedure is analogous in the case of the other summary products) for the mineral olivine in the 0444_4 (low resolution) dataset. The 0232_2 (medium resolution) and 3047_5 (high resolution) overlapping datasets underwent the same process. All three datasets were overlapped in the end to determine the best region to extract spectra from.

Images of the effects the preprocessing has on the data are shown alongside spectra of a chosen pixel within a crater. The images shown are from the 1.8002μm channel of SWIR1, so chosen because it displays distinguishable spectral variation, although all corrections take place on all wavelengths simultaneously.

Obtaining absolute reflectance images

1. The geographic (.NAV) and spectral (.QUB) data files from dataset 0444_4 were calibrated with SOFT05 to obtain images and information of the radiance, geographic information (geocube), the solar spectrum and elevation of the full scene. As mentioned in Section 2.1.1, the software Alpha was used as an interface to SOFT05.
2. The radiance image file (.jdat extension) was inspected for the default bad bands resulting from the calibration with SOFT05.
    - VNIR's 96 bands were all good.

  - SWIR1 had 124 good bands (from 128).
  - SWIR2 had 126 good bands (from 128).

3. The radiance image file was split into three different image sub-datasets, each consisting of one of the different sensors' ranges (VNIR, SWIR1 and SWIR2) by using a bad band list to mask the unnecessary bands belonging to the other sensors.

4. Noisy bands from each of the split radiance image files were further masked using the 'Mask Noisy Bands' module in PyENVI, which makes use of a user defined threshold in the signal to noise ratio to mask bands below the threshold. The threshold was chosen according to how noisy the bands appeared to be when displayed.

   - VNIR's good bands were reduced to 67 with a masking threshold of 60.
   - SWIR1 had 121 good bands with a threshold of 25.
   - SWIR2 had 73 good bands with a threshold of 25.

5. Each radiance file underwent geocorrection in PyENVI using the geocube file generated by SOFT05 (Figure 3.10a).

6. The geocorrected files underwent a solar illumination correction in PyENVI with the solar spectrum file generated by SOFT05 (Figure 3.10c).

7. Subsequently, the files were atmospherically corrected in PyENVI, effectively converting the image to reflectance values (Figure 3.11a).

8. The atmospherically corrected images were stacked using tie-points. Easily identifiable reflectance features across the spectrum were used as tie-points (Figure 3.12). First VNIR and SWIR1 were stacked (15 tie-points between the $0.9222\mu m$ channel in VNIR (Figure 3.12a and the $0.9406\mu m$ channel in SWIR1 (Figure 3.12b), RMSE ≈ 0.3287), and then VNIR + SWIR1 were stacked with SWIR2 (20 tie-points between the $2.6310\mu m$ channel in SWIR1 (Figure 3.12c) and the $2.6328\mu m$ channel in SWIR2 (Figure 3.12d), RMSE ≈ 0.432).

9. The single stacked image was smoothed with a hyperspectral median filter in PyENVI. The filter chosen makes use of the values of the pixels directly in contact with each pixel being averaged, i.e. to the front and back of the pixel (Y dimension), to the left and right (X dimension), and the pixel values directly above and below in the spectral dimension. The result of applying this filter is a reflectance image with edges preserved while noise is smoothed out (Figure 3.11c).

Using summary products

10. Separately, the stacked atmospherically corrected image (prior to median filtering) was used for the application of PyENVI's 'Summary Products'

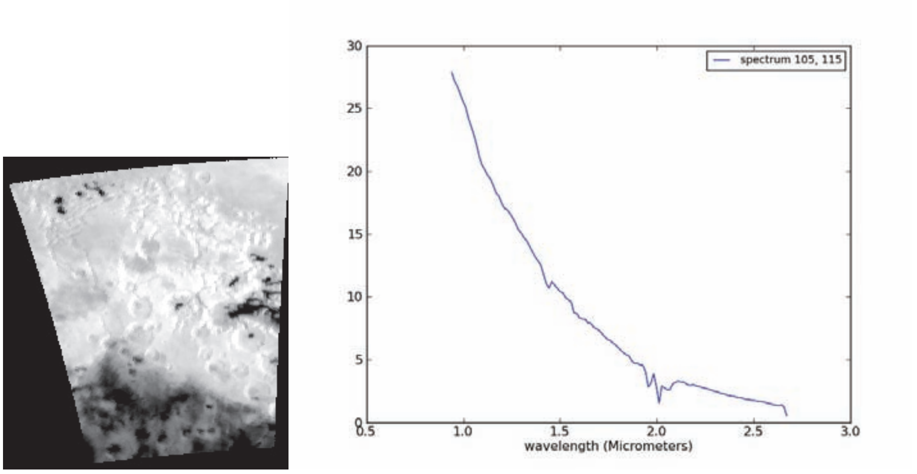

(a) Geocorrected image.

(b) Geocorrected spectrum.

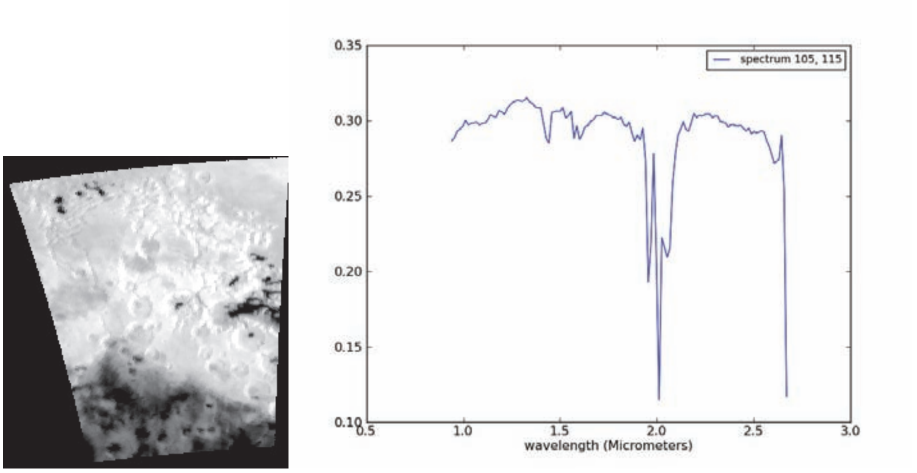

(c) Solar corrected image.

(d) Solar corrected spectrum.

Figure 3.10: The effects of the preprocessing stages on the SWIR1 data subset. The image shown is from the $1.8002 \mu m$ channel.

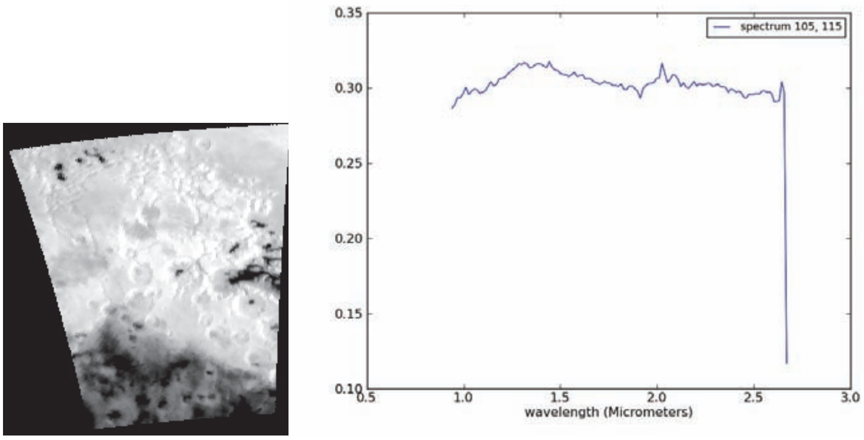

(a) Atmospherically corrected image.

(b) Atmospherically corrected spectrum.

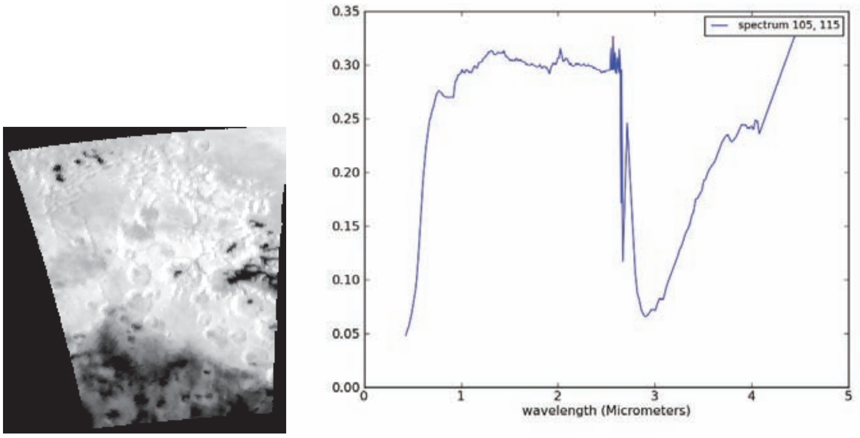

(c) Median filtered image.

(d) Median filtered spectrum, post-stacking.

Figure 3.11: The effects of the preprocessing stages on the SWIR1 data subset. The image shown is from the $1.8002\mu m$ channel.

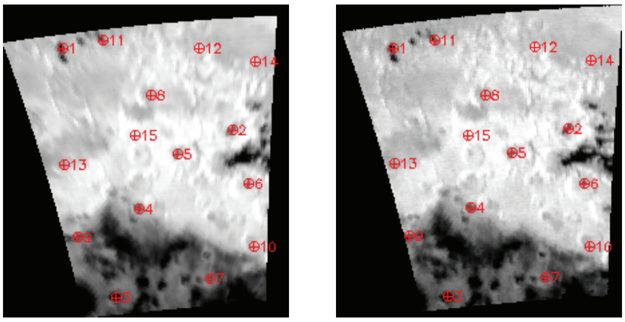

(a) Tie-points in VNIR for warping to SWIR1.

(b) Tie-points in SWIR1 for VNIR to warp to.

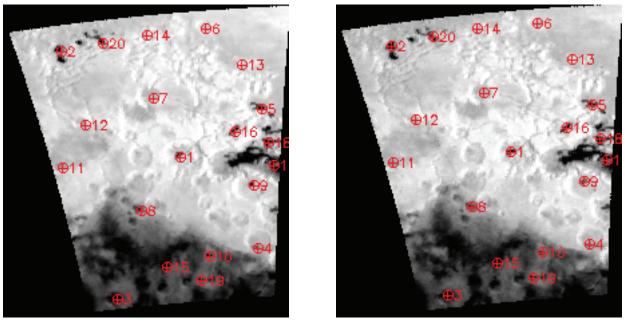

(c) Tie-points in SWIR1 for SWIR2 to warp to.

(d) Tie-points in SWIR2 for warping to VNIR + SWIR1.

Figure 3.12: Tie-points used for the warping and stacking of ORB0444_4.

program. In preparation for this, a normalisation of the image using log residuals was applied (Figure 3.13a). A sharp ascent in the spectrum is apparent between the VNIR and SWIR1 which could be due to the small error from correcting the spatial shift between the sensors, or most probably, due to the persisting calibration problems.

11. Hyperspectral median filtering was applied to the stacked, corrected and normalised image (Figure 3.13c).
12. After the median filtering, the continuum was removed from the spectra of the images, a step necessary for the hydrated minerals summary products (Figure 3.14a). However, noise still persists between SWIR1 and SWIR2 due to the overlapping spectral range (Figure 3.13a). This noise was later removed from the spectra manually by omitting the affected wavelengths.
13. The summary products program was used (Figure 3.14c).

Determining olivine regions of interest

14. Statistics from the OLINDEX scene were studied to find the values of the highest (brightest) 2% of values. These were found to be values between 0.013324 (97.9426%) to 0.048034 (100%).
15. Pixels between the aforementioned values were grouped in as regions of interest (ROIs).
16. The ROIs were draped over the absolute reflectance image of the same scene (Figure 3.15a).

Extracting olivine spectra

Datasets 0232_2 and 3047_5 underwent the same process described for 0444_4 and also have the highest 2% of OLINDEX values in their respective scenes delimited by ROIs (Figures 3.15b and 3.15c).

17. Finally, spectra were extracted from the ROIs (Figure 3.16) that were overlapping in all three scenes and presented spatial coherence (i.e. grouped pixels), indicating spectral stability between them and a possible relationship between the reflectance, mineralogy and geomorphology (Figure 3.17).

3.3 Results of the cross-validation of extracted endmember spectra with spectral angles

The spectral angle was calculated between the extracted spectra from the ROIs in each image resolution against those from the other resolutions. The results can

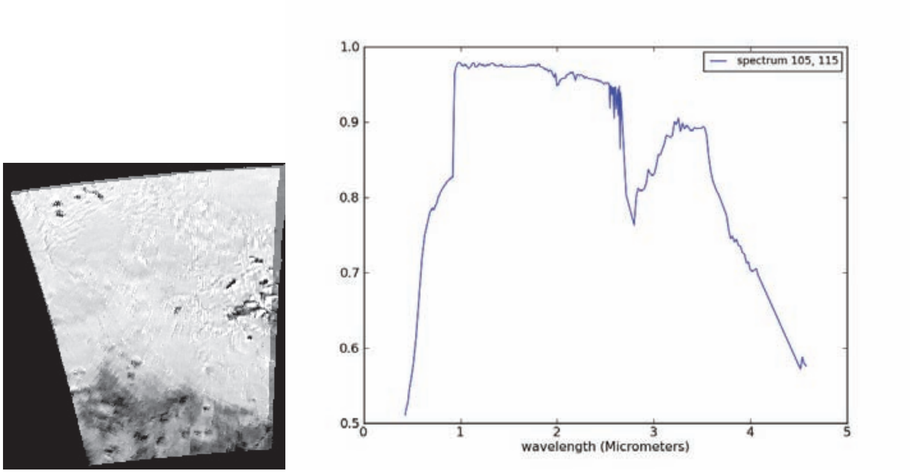

(a) Log residuals applied to stacked dataset

(b) Stacked dataset spectrum after log residuals

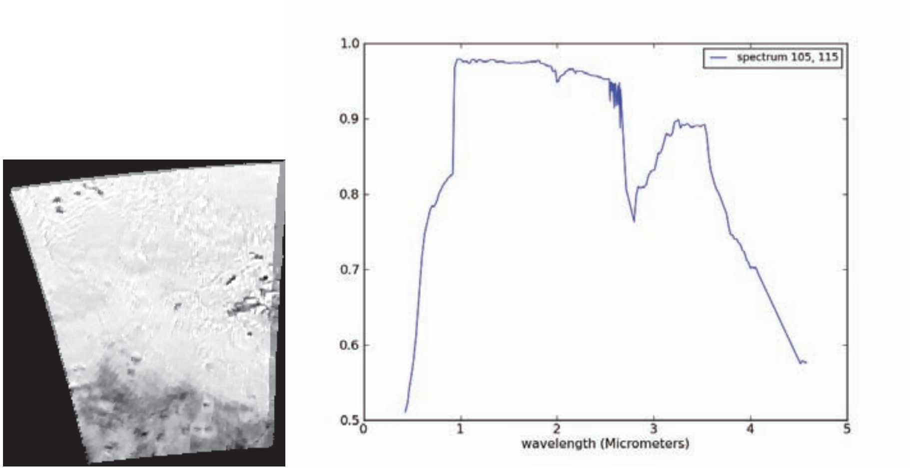

(c) Image after log residuals and median filtering

(d) Spectrum after log residuals and median filtering

Figure 3.13: The effects of the preprocessing stages on the SWIR1 data subset. The image shown is from the $1.8002\mu m$ channel.

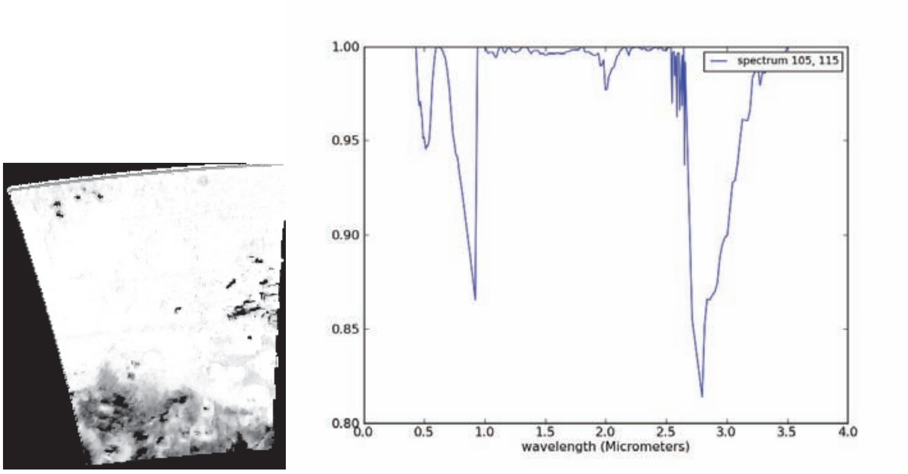

(a) Continuum removed image in preparation for hydrated minerals summary products

(b) Continuum removed spectrum

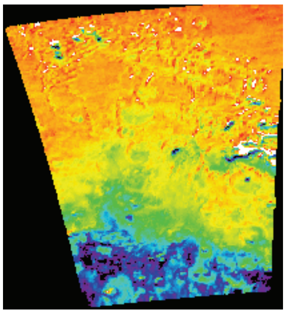

(c) Image of the OLINDEX summary product applied to the scene

Figure 3.14: The effects of the preprocessing stages on the SWIR1 data subset. The image shown is from the 1.8002μm channel. In Figure 3.14c, white represents high values and black represents low values in a red to blue "rainbow" contrast stretch.

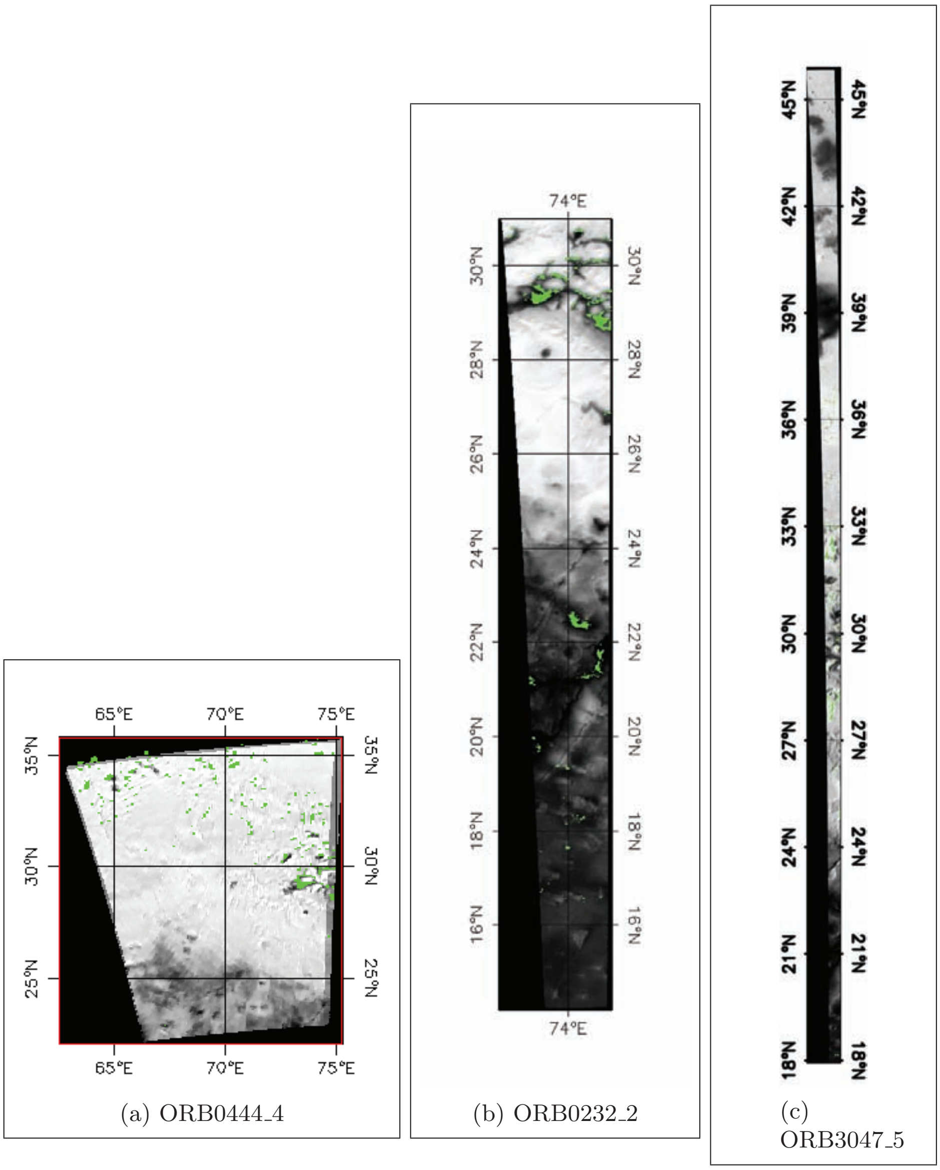

(a) ORB0444_4

(b) ORB0232_2

(c) ORB3047_5

Figure 3.15: Reflectance images with regions of interest (ROIs, in green) of the highest 2% of OLINDEX values.

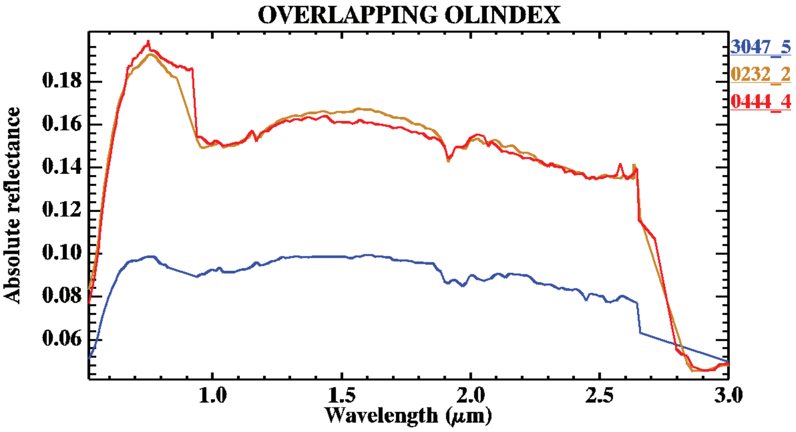

Figure 3.16: Example of olivine spectra extracted from the overlapping ROIs. Plot has been focused on the spectral range where olivine is best identified from.

be found in table 3.1. Spectral angle is a measure of correlation as detailed in Section 2.3. The spectral angle was also calculated between the spectra extracted for different endmembers from the same image they were extracted from to compare how similar or different the spectra are for what should be different mineralogical spectral signatures. The results of this can be found in table 3.2.

3.4 Results from cross-validation between OMEGA and CRISM

The spectral angle between each extracted OMEGA endmember spectrum and the spectrum extracted for the same endmember in CRISM was calculated (Table 3.3). To understand how distinguishable extracted endmember spectra in CRISM were from each other, the spectral angles and similarity percentages were calculated between extracted spectra between different endmembers (Table 3.4). CINDEX could not be calculated for CRISM because of a calibration error occurring in the wavelength range needed to calculate the parameter (around $3.95\mu m$), and causing the reflectance in these wavelengths to be too high. This range was omitted when comparing the OMEGA and CRISM spectra.

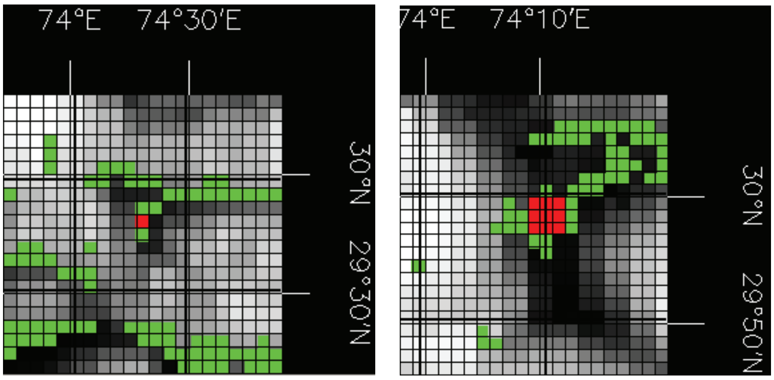

(a) ORB0444_4 (b) ORB0232_2

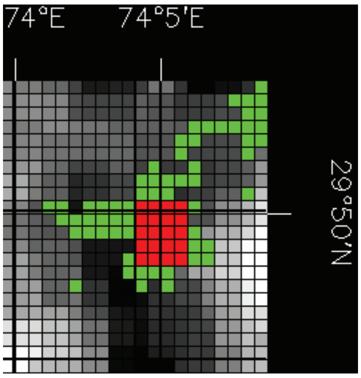

(c) ORB3047_5

Figure 3.17: Overlapping regions where olivine spectra were extracted from. Green pixels are high olivine ROIs; red pixels are the overlapping regions.

Table 3.1: Comparison of spectral angles (θ, in radians) between extracted endmember spectra in each resolution and the spectra extracted for the same endmember in different resolutions.

	ORB3047_5	ORB0232_2	ORB0444_4
OLINDEX			
ORB3047_5	0	0.1133	0.2411
ORB0232_2		0	0.1655
ORB0444_4			0
LCPINDEX			
ORB3047_5	0	0.0476	0.1237
ORB0232_2		0	0.1689
ORB0444_4			0
HCPINDEX			
ORB3047_5	0	0.0495	0.2042
ORB0232_2		0	0.2138
ORB0444_4			0
CINDEX			
ORB3047_5	0	0.0992	0.0971
ORB0232_2		0	0.0960
ORB0444_4			0
D2300			
ORB3047_5	0	0.0558	0.0895
ORB0232_2		0	0.1088
ORB0444_4			0
D2400			
ORB3047_5	0	0.06119	0.1096
ORB0232_2		0	0.2327
ORB0444_4			0

Table 3.2: Comparison of spectral angles (θ, in radians) between extracted endmember spectra in each resolution and spectra extracted for different endmembers in the same resolution.

	olindex	lcpindex	hcpindex	cindex	d2300	d2400
orb3047_5						
olindex	0	0.12	0.05	0.49	0.14	0.04
lcpindex		0	0.07	0.37	0.03	0.09
hcpindex			0	0.44	0.09	0.02
cindex				0	0.35	0.46
d2300					0	0.11
d2400						0
orb0232_2						
olindex	0	0.06	0.02	0.46	0.08	0.03
lcpindex		0	0.06	0.43	0.05	0.07
hcpindex			0	0.48	0.10	0.02
cindex				0	0.39	0.48
d2300					0	0.10
d2400						0
orb0444_4						
olindex	0	0.07	0.09	0.26	0.07	0.06
lcpindex		0	0.04	0.22	0.06	0.04
hcpindex			0	0.21	0.09	0.04
cindex				0	0.23	0.21
d2300					0	0.06
d2400						0

Table 3.3: Spectral angles (radians) between the extracted OMEGA and CRISM spectra.

		CRISM				
		olindex	lcpindex	hcpindex	d2300	d2400
OMEGA	olindex	0.10				
	lcpindex		0.07			
	hcpindex			0.11		
	d2300				0.08	
	d2400					0.11

Table 3.4: Spectral angles (radians) between the extracted spectra from CRISM.

	olindex	lcpindex	hcpindex	d2300	d2400
olindex	0.00	0.08	0.03	0.10	0.03
lcpindex		0.00	0.06	0.03	0.07
hcpindex			0.00	0.07	0.07
d2300				0.00	0.08
d2400					0.00

3.5 Results from the comparison of OMEGA and library spectra

Spectral angles were calculated between the extracted spectra in each OMEGA image and a host of selected mineral spectra from the USGS spectral library measured under laboratory conditions corresponding to the mineralogical signatures the spectral identification and extraction method targeted. The selected minerals are detailed in Table 3.5. Table 3.6 contains the results of comparison between library spectra and extracted spectra in image ORB3047_5. Likewise, Tables 3.7 and 3.8 contain the same for images ORB0232_2 and ORB0444_4, respectively.

Table 3.5: Summary products and their related minerals.

Name	*Abbreviation*[1]	*Mineral group*	*Summary product*
Olivine	Ol	Olivine group; Fe and/or Mg nesosilicate	OLINDEX
Hypersthene/ Orthopyroxene	Opx	Pyroxene group; Fe and Mg inosilicate	LCPINDEX
Diopside	Di	(Clino)Pyroxene group; Mg and Ca inosilicate	HCPINDEX
Pigeonite	Pgt	(Clino)Pyroxene group; Fe, Mg, and Ca inosilicate	HCPINDEX
Calcite	Cal	Carbonate; Ca rich	CINDEX
Serpentine (Lizardite)	Srp	Serpentine group; Fe, Mg phyllosilicate	D2300
Jarosite	Jar	Sulphate; K, Fe rich	D2400

[1] Abbreviations as suggested by [26], excepting jarosite.

3.6 Results of spectral angle mapping

A spectral library was built for each image with the spectra extracted from their respective images as endmembers. Spectral angle mapping was successful in automatically mapping large regions of the OMEGA images with the given endmembers

Table 3.6: Spectral angles (radians) between high resolution ORB3047_5 endmember spectra and laboratory mineral spectra.

ORB3047_5	**Ol**	**Opx**	**Di**	**Pgt**	**Cal**	**Srp**	**Jar**
OLINDEX	0.34	0.18	0.15	0.11	0.12	0.17	0.14
LCPINDEX	0.36	0.18	0.18	0.12	0.13	0.19	0.16
HCPINDEX	0.35	0.19	0.17	0.12	0.11	0.17	0.15
CINDEX	0.34	0.16	0.20	0.15	0.20	0.25	0.10
D2300	0.36	0.18	0.18	0.13	0.13	0.19	0.14
D2400	0.37	0.21	0.18	0.13	0.10	0.16	0.19

Table 3.7: Spectral angles (radians) between medium resolution ORB0232_2 endmember spectra and laboratory mineral spectra.

ORB0232_2	**Ol**	**Opx**	**Di**	**Pgt**	**Cal**	**Srp**	**Jar**
OLINDEX	0.35	0.22	0.18	0.14	0.14	0.20	0.19
LCPINDEX	0.34	0.16	0.18	0.13	0.17	0.23	0.12
HCPINDEX	0.34	0.20	0.17	0.13	0.14	0.20	0.17
CINDEX	0.34	0.17	0.20	0.16	0.21	0.27	0.10
D2300	0.34	0.18	0.18	0.13	0.16	0.22	0.13
D2400	0.34	0.19	0.17	0.13	0.14	0.20	0.15

Table 3.8: Spectral angles (radians) between low resolution ORB0444_4 endmember spectra and laboratory mineral spectra.

ORB0444_4	**Ol**	**Opx**	**Di**	**Pgt**	**Cal**	**Srp**	**Jar**
OLINDEX	0.38	0.26	0.22	0.20	0.21	0.27	0.21
LCPINDEX	0.35	0.21	0.21	0.17	0.21	0.28	0.17
HCPINDEX	0.35	0.22	0.21	0.18	0.22	0.29	0.16
CINDEX	0.36	0.21	0.26	0.24	0.31	0.37	0.10
D2300	0.37	0.21	0.20	0.17	0.19	0.26	0.18
D2400	0.36	0.23	0.21	0.18	0.21	0.28	0.18

3.18a, though only about half the CRISM image was mapped 3.18b The CRISM spectral library did not, however, contain spectra extracted with the CINDEX summary product (see Section 3.3). Some areas of the images did not belong to any of the endmember classes according to the mapping technique (the spectral angle between the image and the endmember spectra was over 0.1), and were therefore unmapped.

The common characteristic to all the images was the mapping of the CINDEX endmember spectra versus the remaining endmembers. In all image resolutions, the areas classified as CINDEX were coherent between images (coherence exists when geographical locations where the same endmember is prevalent regardless of the resolution) whereas the areas classified as the other endmembers were not. This gave rise to a North-South divide of classified patches across an East-West line centred around 25^o N, where regions in the North were mostly CINDEX whereas the classified areas in the south were varied endmembers, not always spatially consistent between resolutions (Figure 3.19a). Continuous classified regions also tended to follow geomorphological features (e.g. crater rims, mountains and valleys, Figure 3.19b)

3.6.1 Results of the visual interpretation of the reflectance spectra

The candidate minerals selected from the USGS spectral library visually according to the position and depth of their features were barite (a barium sulphate, for both CINDEX and LCPINDEX spectra) a hematite (2%) and quartz (98%) intimate mix (an iron oxide and silica, for both CINDEX and LCPINDEX), pyrrhotite (an iron sulphide, for CINDEX) and pigeonite (a high calcium pyroxene, for LCPINDEX). As such, visual comparison of all the USGS library spectra with the extracted CINDEX and LCPINDEX spectra showed that the minerals which best matched the extracted spectra were not what the summary products were meant to identify (Figures 3.20 and 3.21). Calculation of the spectral angles between the candidate minerals and the extracted spectra were smaller in all cases (Table 3.9, meaning that the summary products do *not* serve their intended purpose in this case and that they cannot substitute visual interpretation and identification of spectral features.

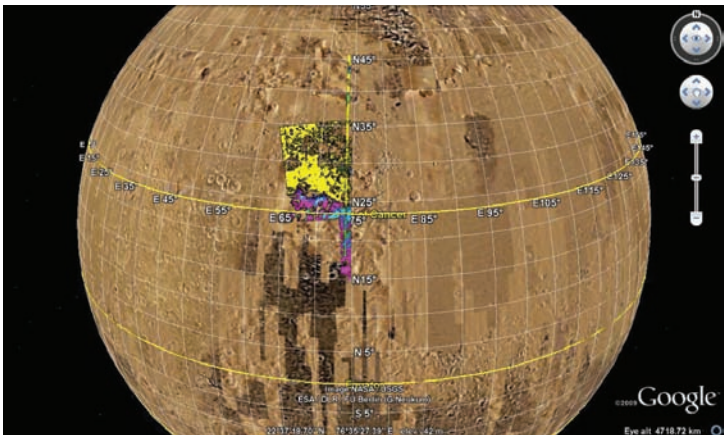

(a) Image of the whole extent mapped

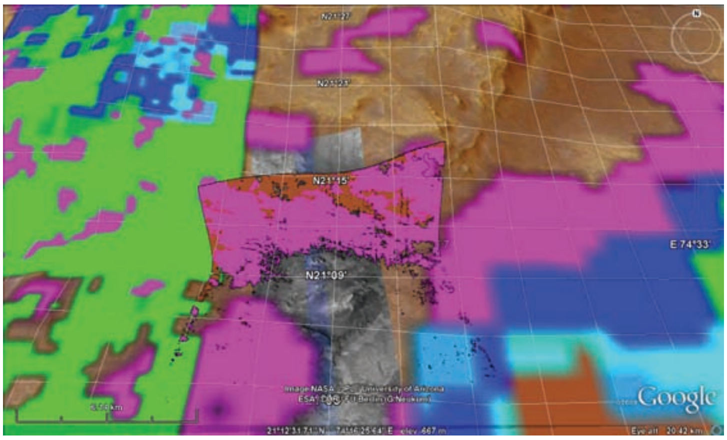

(b) The mapped portion of the CRISM (centre) partially overlapping on ORB3047_5 (right) and fully contained by ORB0232_2 (left).

Figure 3.18: OMEGA and CRISM spectral angle maps overlayed on Google Earth/Mars. Green: OLINDEX, cyan: LCPINDEX, blue: HCPINDEX, yellow: CINDEX, brown: D2300, magenta: D2400.

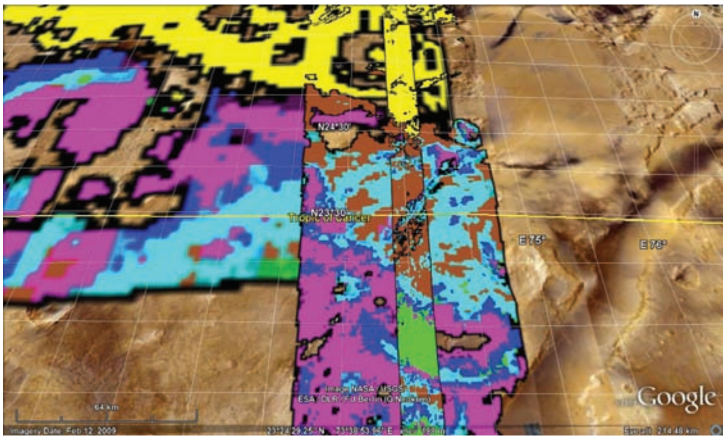

(a) N-S divide of CINDEX versus other endmembers

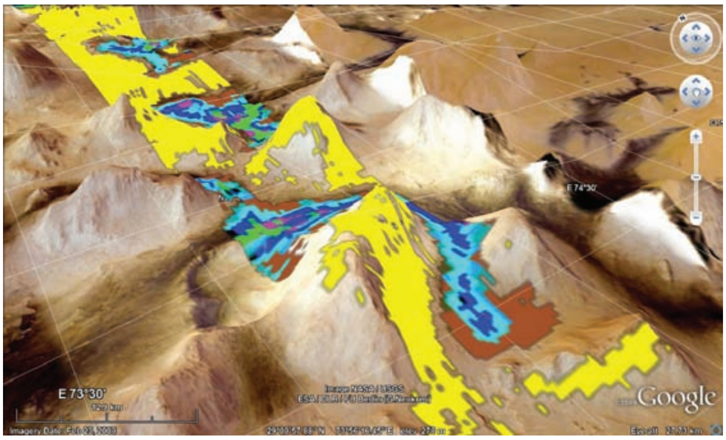

(b) CINDEX on mountains and other endmembers in valleys

Figure 3.19: Details of the spectral angle maps overlayed on Google Earth/Mars. In 3.19a, patches of CINDEX in the North are coherent across resolutions and patches of LCPINDEX in the South are sometimes coherent (occurring in the same geographical areas) between 3047_5 and 0232_2. Overlayed images have black borders to highlight the overlapping resolutions. CINDEX and the other endmembers occupy distinct geomorphological units in the 3047_5 overlay in 3.19b. Vertical exaggeration ×3.

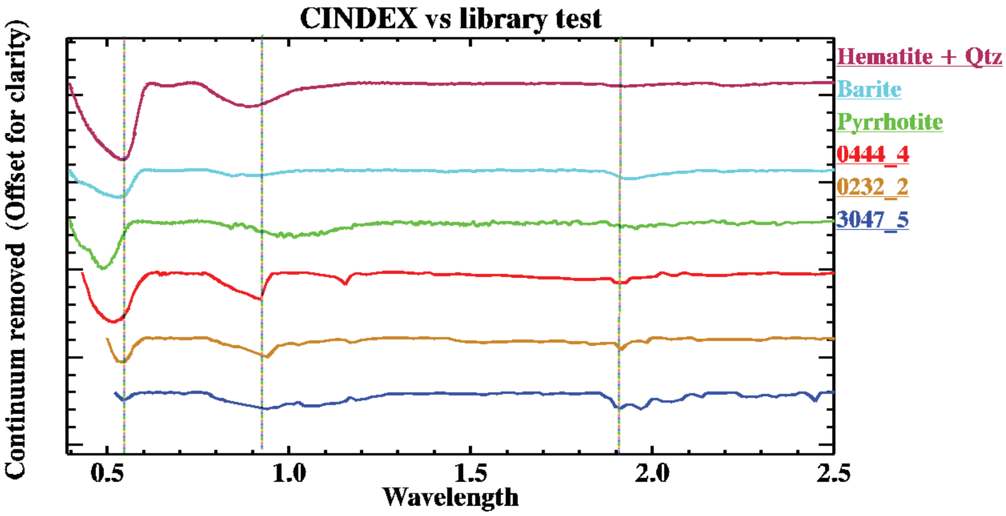

(a) Continuum removed and stacked spectra.

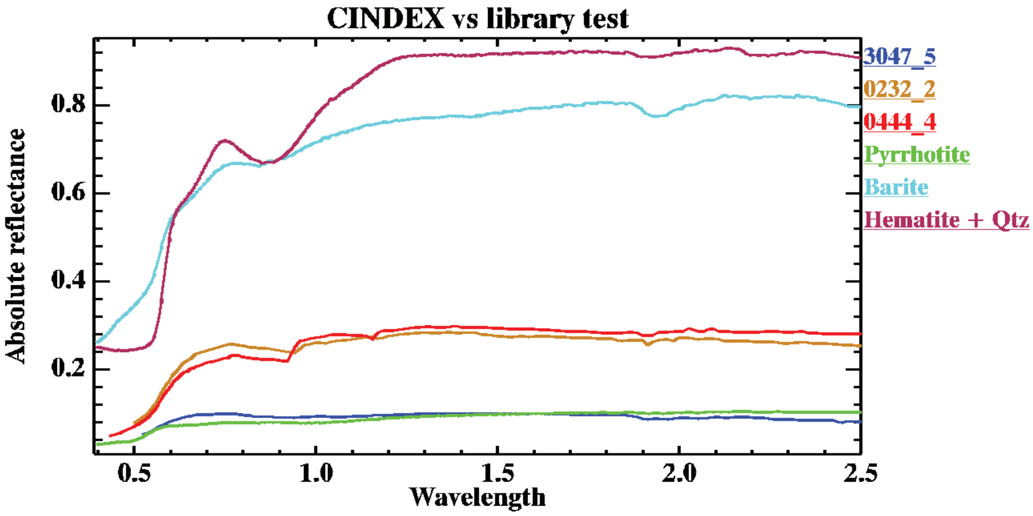

(b) Absolute reflectance

Figure 3.20: Visual comparison of the position and depth of features from extracted CINDEX spectra and similar USGS library spectra.

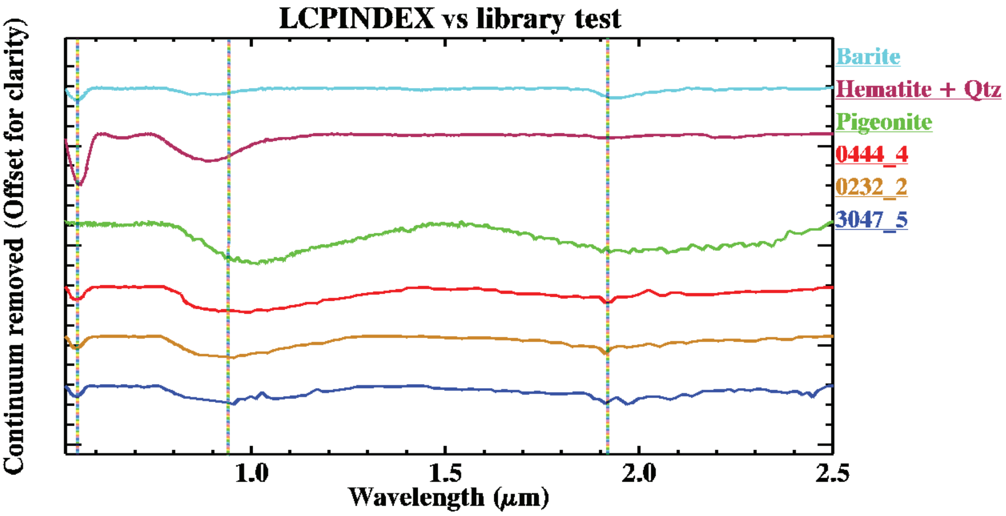

(a) Continuum removed and stacked spectra.

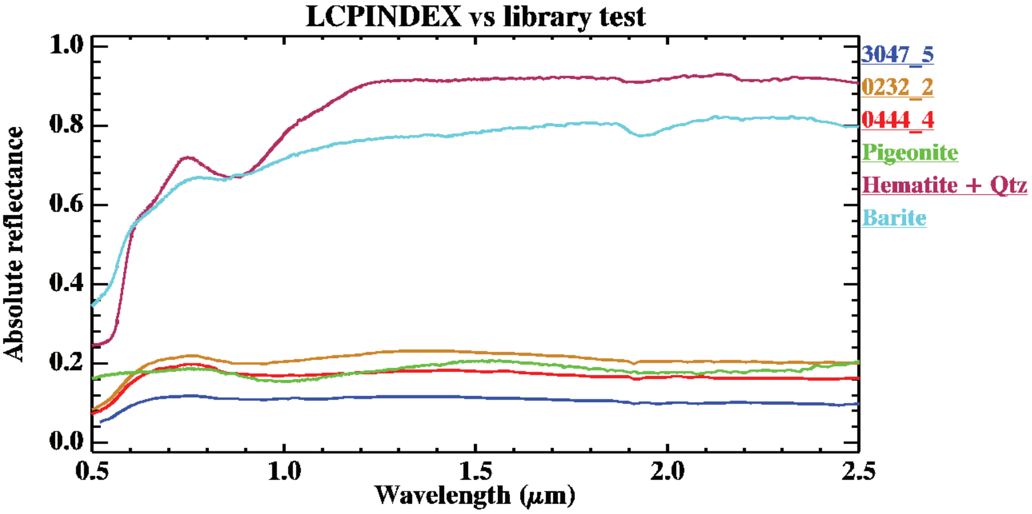

(b) Absolute reflectance

Figure 3.21: Visual comparison of the position and depth of features from extracted LCPINDEX spectra and similar USGS library spectra. Dashed vertical lines indicate the centre position of features used to visually compare library spectra and extracted spectra.

Table 3.9: Spectral angles (in radians) between the spectra extracted with summary products and visually selected spectra from the USGS spectral library.

	3047_5	0232_2	0444_4
CINDEX			
Barite	0.07	0.07	0.08
Hematite + Qtz	0.06	0.09	0.04
Pyrrhotite	0.09	0.11	0.10
LCPINDEX			
Barite	0.14	0.10	0.14
Hematite + Qtz	0.14	0.12	0.18
Pigeonite	0.12	0.13	0.17

Chapter 4

Discussion

The following chapter presents the discussions based on the obtained results in a structured way, following the order of the results presented in Chapter 3. The discussion on the preprocessing and processing stages was presented together in Chapter 3, as the method consisted of an iterative process in which the results (images, regions of interest and spectra) were fed back into the system to obtain the desired final result (an improved OMEGA image processing chain, Section 2.1. The discussions about the remaining results are discussed here.

4.1 Discussion on the results of endmember cross-validation

The spectra extracted using the olivine index differed less between the high resolution image and the medium resolution image (spectral angle $\theta \approx 0.1133$) than between either of the former and the low resolution image ($\theta \geq 0.1655$). Similarity was lowest between the lowest resolution and the highest resolution spectra. However, this was not the case with the other endmember spectra. In the rest of the cases, endmember spectra were slightly more correlated between the low and high resolution images (with the exception of the carbonate index spectra, which were on par, close to 0.09).

On the whole, correlation between the extracted spectra at different resolutions was never below $\theta \approx 0.05$. Reasons for this may be the resolution itself, as mineralogical variability may occur on smaller scales in the sampled regions, accounting for more mixed pixels the lower the resolution. (If this is the case, we would expect higher correlation between high resolution spectra and library spectra (discussed in Sections 3.3 and 4.3).) This does not explain, however, the higher correlation between the high and low resolutions.

A more surprising result was the similarity between different endmember spectra within the same scenes they were extracted from. With the exception of the CINDEX spectra, different endmember spectra within images were highly correlated to each other. This fact could argue that the measured spectral variability is less related to variations within images than the effect different resolutions have on the spectral signature, but the results in table 3.1 indicate that it may not be a causal relationship since correlation between resolutions was generally on the same order as within resolutions.

CINDEX spectra were the only spectra to be distinguishable from the rest, though the spectral angle between the CINDEX spectrum and the rest of the endmember spectra decreased by an average of $0.204\,rad$ in the low resolution.

4.2 Discussion on the results of cross-validation between OMEGA and CRISM

Spectral angle and similarity measured between the CRISM and the OMEGA image revealed that the extracted endmember spectra between them are certainly related (Table 3.3). However, a comparison of endmember spectra within the CRISM image also reveals a low angle and high correlation between their spectra (Table 3.4), even between what should be signatures for very different mineralogies (e.g. D2400/sulphates and OLINDEX/olivine). It may be possible, however, that the high correlation between CRISM endmember spectra may be enhanced by the higher number of channels in CRISM.

A possible reason for this high correlation between spectra may be that sufficient mineralogical diversity does not occur in the small spatial extent of the image and that the method used for selecting and extracting spectra from OMEGA image ROIs cannot be applied with the same weight (i.e. instead of using the highest 2% of values summary product values, the highest 1% may be sufficient) on a CRISM image. This would mean that the selection method actually finds areas with slight spectral variations but which are essentially similar mineralogically.

4.3 Discussion on the results of the comparison of OMEGA and library spectra

It was surprising to see that never did the extracted spectra relate more to the mineral it was supposed to identify than other minerals (with the sole exception of D2400 identifying the sulphate jarosite in the low resolution image).

On the whole, the extracted spectra compared poorly to the library spectra, relative to the correlation found between the extracted spectra of different endmembers themselves (Sections 3.3 and 4.1).

The OLINDEX performed especially poorly in identifying olivine compared to the other indices identifying their respective minerals. In general, the library olivine spectra was as correlated to the spectra extracted for other endmembers as it was for the OLINDEX spectra.

None of the image resolutions had a particular effect on the correlation between each extracted endmember spectrum and its corresponding library spectrum, but the extracted spectra from the high resolution image showed higher similarity to all the library spectra than the spectra from the medium resolution image did, which in turn showed higher correlation with library spectra than the low resolution image did. This might be the result of extracting less clear spectra (more mixed spectra pixels containing higher mineralogical variability) in lower resolutions than in higher ones.

4.4 Discussion on the results of spectral angle mapping

The interpretation of the maps and spatial patterns was seriously restricted due to the high correlation between different endmember spectra shown in previous results. So although the images show seemingly coherent areas that would present common spectral characteristics, the spectra in these areas offer no confidence in identifying the mineralogy by using SAM.

The fact that coherent (i.e. the same endmember is found in the same geographical location across resolutions) classes followed geomorphological features, further indicated that the spectral information relates to mineralogy, though it is still not possible to distinguish specific mineralogical species without e.g. field observations at these geomorphological features to recalibrate OMEGA's orbital observations, a fact which may not occur in the near future. In other words, ancillary information for validation would be decisive.

The effect of shadows artificially creating spectrally cohesive areas cannot be completely overruled, though it was observed that spectrally cohesive areas were found on all faces of mountains, for example.

4.5 Comprehensive discussion of the results

The results shown in this chapter showcased some useful but also some puzzling aspects about the spectral signatures extracted from OMEGA images. To summarise, here follows a list of what was discovered from the results.

1. The modifications (specific noise reduction for each sensor range, minimising the spatial shift between sensors, identifying endmembers with pseudo-reflectance but collecting spectra as absolute reflectance - see section 3.2) to the preprocessing method were a logical step to obtain images and therefore spectra of better quality.
2. The mineralogical spectral signature identification method for OMEGA images based on summary products found spatially coherent areas or patterns in OMEGA images, likely meaning that similar mineral species exist within the areas.
3. These areas were different for each mineral that was attempted to be identified with summary products.

4. However, when compared via their spectral angle, the spectra from these regions appeared very similar (correlated).
5. Could this similarity have been an effect of the spatial resolution? No, there is no strong causal relationship because spectra compared across different resolutions were also very similar.
6. Could this be an uncontrollable calibration problem that affects OMEGA? It is possible; however, a comparison with the newer, higher resolution CRISM instrument shows similar effects.
7. Does the spectral identification method identify the minerals it is supposed to be identifying? A comparison between the extracted spectra and 'pure' laboratory measured spectra shows that this is not the case. Mineralogical mixtures and a surficial dust cover most definitely have an effect, but the spectra sampled from the images formed only a small fraction (2%) of the whole images, consisting of the highest values according to the summary products.
8. The better identification of jarosite by the sulphate index in the low resolution image, relative to the other endmembers is likely not significant because it does not occur in the same geographical position in other resolutions.

From the start, the combined methodology of using summary products to identify candidate regions for spectral sampling plus spectral angle to characterise the spectra against library spectra made logical sense as both summary products and spectral angles identify the trends and curves (the shape) of spectral signatures and place little importance on the actual reflectance magnitude. Summary products did identify spatially distinct regions, though what mineralogical information can be derived from these regions now appears to be an open question. What is clear is that the combined method of applying summary products and spectral angle is not successful at identifying mineralogy.

It could be speculated that the reason for this incompatibility of methods for OMEGA imagery may be because the summary products used to identify spectral signatures place importance on the position and depth of spectral features specific to the minerals being identified via spectral signatures in an image, whereas spectral angle measurements place an equal amount of importance to all points of the spectral curve[1]. Therefore calculation of the spectral angle (and by extension, spectral curve correlation) does not identify minerals because it does not specifically target the characteristic spectral features. Indeed, two very different spectral curves with narrow, precise features in identical positions might form a large spectral angle between them. On the other hand, two otherwise identical spectral curves containing a small number of features in completely different positions might form a low spectral angle between them and score relatively high in correlation.

This hypothesis was briefly tested visually and statistically with OMEGA imagery in a trial and error method (Section 2.7).

---

[1] Dr. F. van Ruitenbeek, personal communication 8th February, 2011.

4.6 Discussion on the results of the visual interpretation of reflectance spectra

The results clearly show that the visual identification of feature depth and position can serve as a method to discriminate between spectra. This was proven when statistics showed that the visually chosen library spectra correlated more with the extracted image spectra, meaning that it was more effective than using summary products.

A information search also reveals that the visually selected minerals from the library spectra have been detected on Mars by a number of different probes and sensors. Pigeonite was detected in a Martian meteorite[2] and the iron oxide hematite is well-known to be present on the Martian surface in the form of dust, but also nodular concretions [28]. Pyrrhotite was also found by the NASA's Viking landers[3].

Previous finds of the minerals also lend some credibility to the fact that the OMEGA images do contain sufficient spectral information to discriminate between some minerals, but that the method of extracting spectra from the image was wrong. A discussion on new methodological considerations follows in Chapter 5.

---

[2] http://www.mindat.org/loc-106227.html, last accessed 15^{th} February, 2011.

[3] http://www.mindat.org/min-4029.html, last accessed 15^{th} February, 2011.

Chapter 5

Conclusions

This final chapter summarises the main findings of the research undertaken in this thesis and recommends on how to proceed with research on mineral characterisation of the surface of Mars via remote sensing.

Research was undertaken to study the stability of reflectance spectra acquired by the hyperspectral OMEGA spectrometer on ESA's Mars Express satellite and to identify the mineralogy of the surface of Mars using this data. The method consisted of an initial preprocessing stage to obtain clean reflectance images as free as possible from noise and interferences. The method to identify the surface mineralogy involved the use of summary products, indices based on the spectral characteristics of general mineral groups that are meant to locate regions where such minerals are to be found. Subsequently, spectra extracted from regions pinpointed by the summary products served as endmembers in a spectral library for each image studied, containing spectra of six important rock-forming groups of minerals found on the surface of Mars, according to the literature.

The spectral libraries were used for spectral angle mapping, where the spectra in the library corresponding to different mineral groups (according to spectra extracted from the images with the summary products) were statistically matched against the spectra in the images being mapped. Some spatial coherence of the distribution of minerals was observed in the maps.

Unfortunately, statistical matching (via the spectral angle) of the extracted spectra with summary products against mineral spectra observed in laboratory conditions (the USGS spectral library) showed that the method failed to relate the spectra. Moreover, the spectral angles between different endmembers as well as between different spatial resolutions were low, proving a high correlation existed between spectra extracted for different summary products as well as between different images. The exception to this was the identification of the sulphate jarosite by the sulphate index (D2400) in the low resolution image. This does not indicate that jarosite was present but a higher probability of its presence because of a higher correlation between extracted and library spectra. Considering that the higher correlation was not found across resolutions, the confidence for its detection remains low.

To see whether the high correlation between spectra of different endmembers was exclusive to OMEGA, a cross-validating test was carried out by comparing the spectra extracted from OMEGA imagery with summary products to spectra extracted with summary products from images acquired by the CRISM hyperspectral spectrometer on NASA's Mars Reconnaissance Orbiter. Tests showed that the high correlation between extracted spectra persisted in CRISM images, and that they did not correlate well with laboratory measurements either.

The method failed to map precise mineralogical species because the summary products did not identify the spectral characteristics of the minerals they claim to identify. To test whether this was the cause of the failure, a trial and error or "brute-force" approach, in which all the laboratory-sampled mineral spectra available in the USGS spectral library were visually compared to the spectra extracted from the OMEGA images with summary products. The spectral angles were calculated between the image extracted spectra and the spectra of minerals selected from the spectral library which visually matched the position and depth of the image extracted spectra. In all cases, these angles were lower than the angles calculated between the spectra extracted with summary products and the minerals they were supposed to identify. The minerals that formed lower spectral angles with the spectra extracted with summary products did not belong to the mineralogical groups the summary products were meant to identify (e.g. the carbonate index (CINDEX) summary product was more akin to a mix of hematite (an iron oxide) and quartz than to calcite (calcium carbonate), Figure 3.20 and Table 3.9.).

In conclusion, the chosen spectral summary products are not able to identify mineralogy with confidence.

5.1 Recommendations

Future studies in mineralogical characterisation of the Martian surface with hyperspectral information should draw from the lessons learnt in this research, namely that the current mineralogical parameters or summary products do not pass the statistical test and should therefore be used with care and definitive prior knowledge of the probable mineralogical distribution and species in the images.

It is tempting to blame the instruments and their calibration for the bad data received and suggest that orbiting spectrometers in future missions incorporate some form of recalibration that could be carried out periodically or when necessary while in orbit, in order to minimise the effects of the trip to Mars on the signal and the deterioration due to cosmic radiation in time. However, as mentioned previously, there are no plans in the near future to insert orbiters containing hyperspectral spectrometers into Martian orbit, so there is no option but to make the best out of the otherwise abundant data available.

In order to minimise the effect of the large pixel size on the spectra, it would be practical to use CRISM for mineralogical characterisation instead of OMEGA. Authors (see section 1.1.2) have worked on unmixing models for OMEGA, but these should be adapted for CRISM. The idea of extracting spectra to build a spectral library of endmembers used to map the images is in itself a flawed method in this case, since by using spectral angles, the spectra extracted cannot correlate to the mineralogical spectra that we do have a knowledge of (gathered, for example, in spectral libraries of laboratory measured mineral spectra). Maps classified using only image spectra here are ‘artificial’ in the sense that some subtle spectral variation can be identified, but precise mineralogical species cannot.

But the question of which minerals should form the spectral library of possible minerals found remains. We cannot blindly use a large amount of mineralogical spectra, even though the trial and error “brute-force” approach (using all the mineral spectra in the spectral library) carried out in this thesis (sections 2.7) demonstrated that it was more effective at finding minerals than the summary products. The scientific merit of a trial and error approach in this case is somewhat debatable: a large number of mineral spectra in the library is useful because there is a higher chance that a high correlation between image spectra and some mineral spectra; however without prior evaluation of the mineralogy possibly present in the region being mapped, a similar correlation method might identify distributions of minerals in space which do not make geologic sense after interpretation (typifying the adage ‘Garbage in, garbage out’), e.g. high grade metamorphic minerals and unaltered carbonates side by side, barring tectonic activity bringing them close together. This possibility exists, though how probable it is is a matter of debate. The chances of this situation occurring rise when the number of minerals (equally weighted in their probability of occurrence, e.g. determined by the minimum spectral angle) included in the library rises.

A solution to the choice of minerals for the spectral library might lie in very promising research being undertaken by NASA’s Mars Exploration Rovers (MERs) since 2004[1]. These are the only existing sources of ‘ground truth’, and the minerals they have detected are likely perfect candidates for a cautious yet scientific and proof-based spectral library for the analysis of CRISM images.

The mineralogical diversity discovered by the rovers with the Mini Mössbauer Spectrometer (MIMOS II), Mini-Thermal Emission Spectrometer (Mini-TES) and Athena’s Alpha-Particle-X-Ray Spectrometer (APXS) has been exciting; notably, their landing sites had been mineralogically mapped and characterised using OMEGA and CRISM, but the findings of the rovers completely contradicted the interpretations made by using the orbiting spectrometers [28]. What was thought to be materials of sedimentary phyllosilicate origin (Gusev crater) were in fact igneous/ volcanic mafics in nature, as seen by Spirit rover [25], whereas materials thought to be igneous mafics (Victoria crater) proved to be sedimentary in origin by the Opportunity rover [28].

The future of science missions to Mars relies heavily on landers and rovers, with NASA’s Mars Science Laboratory (MSL, “Curiosity”) set to be launched in 2011 [14], and the joint ESA/NASA ExoMars missions to be launched in 2016 and 2018 [30], with the not-so-distant final objective of returning samples to Earth.

---

[1] http://marsrovers.nasa.gov/overview/ last accessed: 15^th February, 2011.

Though the main science objective of the rovers is to find traces of past and/or present life, mineralogy is crucial in determining where these traces of life may be. (Current consensus is that the rovers must target sites with phyllosilicates as well as sites where hydrothermal activity occurred.) Landers must deploy their rovers relatively close to these sites as the autonomy of the rovers is an important limitation [28].

So mapping the mineralogical distribution from orbit would greatly aid in selecting landing sites for rovers, directly influencing where the search for traces of life occurs. But the MER experience showed that the interpretation of orbital data was wrong [28].

In short, learning from my mistakes as well as from the planetary science community's, I suggest the following for future mineralogical mapping of the surface of Mars from the data of the current instruments:

1. Favour CRISM imagery rather than OMEGA images. Even if it is regarded that OMEGA is useful for mapping large areas, mineralogical mixes, dust, noise and interferences are likely worse in OMEGA and can be avoided to some extent with CRISM. Mosaics can be built for extended regional maps should they be necessary.
2. Be certain that images are corrected: striping persists in CRISM images. This means the pre-processing method designed and modified here for OMEGA might have to be reviewed for CRISM, which is a feasible task given the experience gathered from this project.
3. Build a spectral library of minerals identified by the rovers' instruments (meaning there is no "garbage in"). This might not be initially intuitive since there must be a resampling of the bands. However, the discovered minerals are documented together with their locations.
4. Use the spectral library as endmembers for mapping (e.g. via spectral angle, a flexible (because magnitude is not important) yet rigorous (because spectral shape is important) correlation method on CRISM images corresponding to where the minerals were identified by the rovers, creating a link between CRISM and the MER instruments. Further mapping can be done on areas unexplored by the rovers after this stage.

References

[1] W. H. Bakker and K. S. Schmidt. Hyperspectral edge filtering for measuring homogeneity of surface cover types. *ISPRS Journal of Photogrammetry and Remote Sensing*, 56(4):246–256, July 2002.

[2] W.H. Bakker. *PyENVI User Manual.* ITC Netherlands, October 2010.

[3] W.H. Bakker, F.J.A. van Ruitenbeek, and H.M.A. van der Werff. Processing OMEGA hyperspectral imagery for mineral mapping of the Nili Fossæ area on Mars, September 2009.

[4] Jean-Pierre Bibring, Yves Langevin, Aline Gendrin, Brigitte Gondet, François Poulet, Michel Berthé, Alain Soufflot, Ray Arvidson, Nicolas Mangold, John Mustard, P. Drossart, and the OMEGA team. Mars surface diversity as revealed by the OMEGA/Mars Express observations. *Science*, 307(11):1576 – 1581, March 2005.

[5] J.P. Bibring, A. Soufflot, M. Berthé, Y. Langevin, B. Gondet, P. Drossart, M. Bouyé, M. Combes, P. Puget, A. Semery, et al. OMEGA: Observatoire pour la Minéralogie, l'Eau, les Glaces et l'Activité. In *Mars Express: The Scientific Payload*, volume 1240, pages 37–49, 2004.

[6] Michael H. Carr and James W. Head III. Geologic history of Mars. *Earth and Planetary Science Letters*, 294(3-4):185–203, 2010. Mars Express after 6 Years in Orbit: Mars Geology from Three-Dimensional Mapping by the High Resolution Stereo Camera (HRSC) Experiment.

[7] A. Chicarro. Future European exploration of Mars. Presented in the EUROPLANET JRA1 Landing Sites for Exploration Missions, January 2011.

[8] R.N. Clark, G.A. Swayze, R. Wise, E. Livo, T. Hoefen, R. Kokaly, and S.J. Sutley. USGS digital spectral library splib06a: U.S. geological survey, digital data series 231. Technical Report 231, U.S. Geological Survey, September 2007.

[9] J.-Ph. Combe, S. Le Mouélic, C. Sotin, A. Gendrin, J.F. Mustard, L. Le Deit, P. Launeau, J.-P. Bibring, B. Gondet, Y. Langevin, and P. Pinet. Analysis of OMEGA/Mars Express data hyperspectral data using a Multiple-Endmember linear spectral unmixing model (MELSUM): methodology and first results. *Planetary and Space Science*, 56(7):951–975, May 2008.

[10] Bethany L. Ehlmann, John F. Mustard, Scott L. Murchie, François Poulet, Janice L. Bishop, Adrian J. Brown, Wendy M. Calvin, Roger N. Clark, David J. Des Marais, Ralph E. Milliken, Leah H. Roach, Ted L. Roush, Gregg A. Swayze, and James J. Wray. Orbital identification of carbonate-bearing rocks on Mars. *Science*, 322(19):1828 – 1832, December 2008.

[11] ESA. ESA's Rosetta mission science programme. http://sci.esa.int/science-e/www/area/index.cfm?fareaid=13. Last accessed: 12th of February 2011.

[12] European Space Agency. Instrument documentation for OMEGA (INSTRUMENT.CAT). Technical report, Europan Space Agency, September 2004.

[13] Caleb I. Fassett and James W. Head III. Fluvial sedimentary deposits on Mars: Ancient deltas in a crater lake in the Nili Fossae region. *Geophysical Research Letters*, 32(L14201), July 2005.

[14] M. Golombek. Selection of mars landing sites. Presented in the EUROPLANET JRA1 Landing Sites for Exploration Missions, January 2011.

[15] S. Le Mouelic, J.P. Combe, V. Sarago, N. Mangold, M. Masse, J.P. Bibring, B. Gondet, Y. Langevin, and C. Sotin. An iterative least squares approach to decorrelate minerals and ices contributions in hyperspectral images: Application to Cuprite (earth) and Mars. In *Hyperspectral Image and Signal Processing: Evolution in Remote Sensing, 2009. WHISPERS'09. First Workshop on*, pages 1–4. IEEE, 2009.

[16] N. Mangold, F. Poulet, J. F. Mustard, J.-P. Bibring, B. Gondet, Y. Langevin, V. Ansan, Ph. Masson, C. Fasset, J. W. Head III, H. Hoffmann, and G. Neukum. Mineralogy of the Nili Fossae region with OMEGA/Mars Express data: 2. aqueous alteration of the crust. *Journal of Geophysical Research*, 112(E08S04), 2007.

[17] Mars Express/OMEGA team. *OMEGA software (IDL version) release SOFT05 readme file*. ESA, February 2008.

[18] Joseph Michalski, François Poulet, Jean-Pierre Bibring, and Nicolas Mangold. Analysis of phyllosilicate deposits in the Nili Fossae region of Mars: Comparison of TES and OMEGA data. *Icarus*, 206(1):269–289, March 2010.

[19] Joseph R. Michalski and Paul B. Niles. Deep crustal carbonate rocks exposed by meteor impact on Mars. *Nature Geoscience*, 3:751–755, November 2010.

[20] J. F. Mustard, F. Poulet, A. Gendrin, J.-P. Bibring, Y. Langevin, B. Gondet, N. Mangold, G. Bellucci, and F. Altieri. Olivine and Pyroxene Diversity in the Crust of Mars. *Science*, 307(5715):1594–1597, 2005.

[21] J. F. Mustard, F. Poulet, J. W. Head, N. Mangold, J.-P. Bibring, S. M. Pelkey, C. I. Fasset, Y. Langevin, and G. Neukum. Mineralogy of the Nili Fossae region with OMEGA/Mars Express data: 1. ancient impact melt in the Isidis Basin and implications for the transition from the Noachian to Hesperian. *Journal of Geophysical Research*, 112(E08S03), 2007.

[22] S. M. Pelkey, J. F. Mustard, S. Murchie, R. T. Clancy, M. Wolff, M. Smith, R. Milliken, J.-P. Bibring, A. Gendrin, F. Poulet, Y. Langevin, and B. Gondet. CRISM multispectral summary product: Parametrizing mineral diversity on Mars from reflectance. *Journal of Geophysical Research*, 112(E08S14), 2007.

[23] F. Poulet, C. Gomez, J.-P. Bibring, Y. Langevin, B. Gondet, P. Pinet, G. Belluci, and J. Mustard. Martian surface mineralogy from Observatoire pour la Minéralogie, l'Eau, les Glaces et l'Activité on board the Mars Express spacecraft (OMEGA/MEx): global mineral maps. *J. Geophys. Res.*, 112(E8):E08S02, July 2007.

[24] F. Poulet, N. Mangold, D. Loizeau, J.P. Bibring, Y. Langevin, J. Michalski, and B. Gondet. Abundance of minerals in the phyllosilicate-rich units on Mars. *Astronomy and Astrophysics*, 487(2):41–44, 2008.

[25] M.E. Schmidt, W.H. Farrand, J.R. Johnson, C. Schr[U+FFFD]der, J.A. Hurowitz, T.J. McCoy, S.W. Ruff, R.E. Arvidson, D.J. Des Marais, K.W. Lewis, D.W. Ming, S.W. Squyres, and P.A. de Souza Jr. Spectral, mineralogical, and geochemical variations across home plate, gusev crater, mars indicate high and low temperature alteration. *Earth and Planetary Science Letters*, 281(3-4):258–266, May 2009.

[26] J. Siivola and RA Schmid. Systematic nomenclature for metamorphic rocks: list of mineral abbreviations. *Recommendations by the IUGS Subcommission on the Systematics of Metamorphic Rocks*, 2007.

[27] Y. Sohn and N.S. Rebello. Supervised and unsupervised spectral angle classifiers. *Photogrammetric Engineering and Remote Sensing*, 68(12):1271–1282, 2002.

[28] S.W. Squyres. Exploring the Martian surface: Lessons learned from thirteen rover-years on Mars. Presented in the EUROPLANET JRA1 Landing Sites for Exploration Missions, January 2011.

[29] J.N. Sweet. The spectral similarity scale and its application to the classification of hyperspectral remote sensing data. In *Advances in Techniques for Analysis of Remotely Sensed Data, 2003 IEEE Workshop on*, pages 92–99. IEEE, 2004.

[30] J.L. Vago. Landing sites: A project scientist's perspective. Presented in the EUROPLANET JRA1 Landing Sites for Exploration Missions, January 2011.

[31] Harald van der Werff. *ALPHA graphical user interface for OMEGA SOFT05 Software*. International Institute for Geo-Information Science and Earth Observation (ITC), The Netherlands, 2009.

[32] Harald van der Werff, Frank van Ruitenbeek, Tanja Zegers, and Freek van der Meer. Geologic mapping on Mars by segmentation of OMEGA data. In *5th EARSeL Workshop on Imaging Spectroscopy*, Bruges, Belgium, April 2007.

[33] Lorenz Wendt, Jean-Philippe Combe, Patrick C. McGuire, Janice L. Bishop, and Gerhard Neukum. Linear spectral unmixing of near-infrared hyperspectral data from Juventae Chasma, Mars. In Lorenzo Bruzzone, Claudia Notarnicola, and Francesco Posa, editors, *Image and Signal Processing for Remote Sensing XV*, volume 7477, page 74770M. SPIE, 2009.